
White Rose Research Online

eprints@whiterose.ac.uk
https://eprints.whiterose.ac.uk
Universities of Leeds, Sheffield and York

Deposited via The University of Sheffield.

White Rose Research Online URL for this paper:
https://eprints.whiterose.ac.uk/id/eprint/117444/

Version: Accepted Version

Article:
Kim, E. and Hollerbach, R. (2017) Geometric structure and information change in phase transitions. Physical Review E, 95 (6). 062107. ISSN: 1539-3755

https://doi.org/10.1103/PhysRevE.95.062107

Reuse
Items deposited in White Rose Research Online are protected by copyright, with all rights reserved unless indicated otherwise. They may be downloaded and/or printed for private study, or other acts as permitted by national copyright laws. The publisher or other rights holders may allow further reproduction and re-use of the full text version. This is indicated by the licence information on the White Rose Research Online record for the item.

Takedown
If you consider content in White Rose Research Online to be in breach of UK law, please notify us by emailing eprints@whiterose.ac.uk including the URL of the record and the reason for the withdrawal request.



Geometrical structure in phase transition

Eun-jin Kim

School of Mathematics and Statistics,

University of Sheffield, Sheffield, S3 7RH, UK

Rainer Hollerbach

Department of Applied Mathematics,

University of Leeds, Leeds LS2 9JT, UK

Abstract

We propose a toy model for a cyclic order-disorder transition and introduce a new geometric methodology to understand stochastic processes involved in transitions. Specifically, our model consists of a pair of Forward and Backward Processes (FP and BP) for the emergence and disappearance of a structure in a stochastic environment. We calculate time-dependent PDFs and the information length $\mathcal{L}$, which is the total number of different states that a system undergoes during the transition. Time-dependent PDFs during transient relaxation exhibit strikingly different behaviour in FP and BP. In particular, FP driven by instability undergoes the broadening of the PDF with large increase in fluctuations before the transition to the ordered state accompanied by narrowing the PDF width. During this stage, we identify an interesting geodesic solution accompanied by the self-regulation between the growth and nonlinear damping where the time scale τ of information change is constant in time, independent of the strength of the stochastic noise. In comparison, BP is mainly driven by the macroscopic motion due to the movement of the PDF peak. The total information length $\mathcal{L}$ between initial and final states is much larger in BP than in FP, increasing linearly with the deviation γ of a control parameter from the critical state in BP while increasing logarithmically with γ in FP. $\mathcal{L}$ scales as $|\ln D|$ and $D^{-1/2}$ in FP and BP, respectively, where D measures the strength of the stochastic forcing. These differing scalings with γ and D suggest a great utility of $\mathcal{L}$ in capturing different underlying processes, specifically, diffusion vs advection in phase transition by geometry. We discuss physical origins of these scalings and comment on implications of our results for bistable systems undergoing repeated order-disorder transitions (e.g. fitness).

I. INTRODUCTION

Phase transition plays a vital role in many disciplines ranging from cosmology, elementary particle theory, condensed matter, chemistry, biology to social-economic movements [1–5]. In critical phenomena, a set of control parameters such as temperature triggers the transition of a state of matter (e.g. vapour, water and ice) or magnetisation (ferromagnet), leading to the emergence/disappearance of a global mode (macroscopic observable). At a super-critical (disordered) state, the value of an order parameter is zero while at a subcritical (ordered) state, it takes a non-zero value. Order-disorder transition is also at the heart of self-organisation [6] whereby coherent structure spontaneously emerges out of complexity, providing a key mechanism for maintaining dynamic balance in non-equilibrium systems. Examples include the formation of shear flows/vortices in fluids or plasmas [7–12] or pattern formation in chemical oscillators, embryogenesis, and even traffic flows. With improved measurement technology in biological experiments, there has been accumulating evidence that similar transitions play a primary role in different biological processes [4]. For instance, [13] demonstrated an emerging property in whole-genome expression through the transition from a unimodal distribution to a bimodal distribution due to bistability and claimed Self-Organized Criticality (SOC) [14–16].

Bistability, often used as a simple framework to study disorder-order (or supercritical-subcritical), is thought to provide a crucial regulating mechanism in different systems, e.g. in electric circuits [17], in various cellular processes such as cycles, differentiation and apoptosis, regulation of heart, brain, etc [18–23]. One of the most striking attributes of some bistable systems is continuous switching between ordered and disordered states, the transition occurring in bursts interspersed by a quiescent period (e.g. see [18]). Furthermore, the sandpile model – a prototypical model for SOC [14] – can also be viewed as the repetition of such switching between the build-up of large gradients (forcing) and the sandpile's collapse beyond some critical gradient (dissipation). In fact, recent work by di Santo et al [24] attempted to formally adapt SOC to bistable systems by invoking Self-Organized Bistability. Our work was motivated to present a new way of understanding disorder-to-order and order-to-disorder transitions in bistable systems, highlighting asymmetry between these two processes.

In this paper, we propose a toy model for a cyclic order-disorder transition, perform detailed study on the time-evolution of PDFs, and introduce a new geometric methodology to understand stochastic processes involved in order-disorder transition. Specifically, our model consists of a pair of Forward and Backward Processes for the emergence of a structure and its reverse process, the disappearance of a structure, respectively, in a stochastic environment. We calculate time-dependent PDFs and the total number of different states that a system undergoes during the transition. The latter is quantified by the information length [25–29], which is dimensionless, defined as (see Appendix A):

$$\mathcal{L}(t) = \int_0^t \frac{dt_1}{\tau(t_1)} = \int_0^t dt_1 \sqrt{\int dx \frac{1}{p(x,t_1)} \left[\frac{\partial p(x,t_1)}{\partial t_1}\right]^2}, \tag{1}$$

where $p(x,t)$ is a time dependent PDF for a stochastic variable x. In Eq. (1), $\tau(t)$ is the time-varying "time-unit":

$$\frac{1}{[\tau(t)]^2} = \int dx \frac{1}{p(x,t)} \left[\frac{\partial p(x,t)}{\partial t}\right]^2. \tag{2}$$

$\tau(t)$ in Eq. (2) has dimensions of time, and quantifies the correlation time over which the (dimensionless) information changes, thereby serving as the time unit as far as the information is concerned. The first equality in Eq. (1) represents that $\mathcal{L}$ is the total elapsed time measured in units of τ. Alternatively, the information length represents the total different number of states between the initial and final times, 0 and t respectively, and establishes a distance between the initial and final PDFs in the statistical space. Our information length is based on Fisher information (c.f. [30]) and is a generalisation of statistical distance [31], where the distance is set by the number of distinguishable states between two PDFs. While the latter was heavily used in equilibrium or near-equilibrium of classical and quantum systems [32–40], our recent work [25–29] adapted this concept to a non-equilibrium system to elucidate geometric structure of non-equilibrium processes. Specifically, [29] mapped out the attractor structure $\mathcal{L}_\infty$ vs x_0 for the linear and cubic process and showed i) that a linear damping preserves a linear geometry $\mathcal{L}_\infty \propto x_0$ and ii) that a nonlinear damping gives rise to a power-law scaling $\mathcal{L}_\infty \propto x_0^n$ ($n \sim 1.5-1.9$) of the attractor structure. [28] found interesting geodesic solutions in a non-autonomous Ornstein-Uhlenbeck (O-U) process by modulating model parameters and by including time-dependent external deterministic killing term. No-

tably, the modulation of the model parameters and the killing term were periodic/oscillatory.

Recalling that a geodesic is a particular path minimising the total information change, it is important to emphasise that it endows a system with the advantage of undergoing the least amount of changes during the non-equilibrium process. This could be extremely beneficial to a system when adjusting to a changing environment takes time and/or is costly. Our previous results summarized above then raise the important question of what basic physical mechanisms are responsible for a geodesic in a more realistic system without tailored time-dependent control. Our previous experience with the cubic process [29] suggests that a nonlinear interaction might be one of them. In this paper, we show that the predator-prey type self-regulation between the positive feedback and the negative feedback in the disorder-to-order transition maintains the system closer to the geodesic, minimising the information change. That is, we find that the self-regulation with a nonlinear interaction facilitates a geodesic.

Motivated by a quenched experiment like a spinoidal decomposition [3], we induce a sudden change of a control parameter at the initial time of Forward and Backward Processes and study the evolution of an initially far-from-equilibrium unimodal PDF into an equilibrium bimodal PDF during disorder-to-order transition in the Forward Process, and vice versa in the Backward Process. From time-dependent PDFs, we calculate the information change associated with a non-equilibrium evolution in Forward and Backward Processes by the information length, highlighting differences. We note that a sudden change in control parameters takes place naturally in self-organised systems, for instance, in gene expressions (e.g. see [18]). We present high-resolution numerical results together with analytical analysis in limiting cases. The remainder of this paper is organized as follows. Section II presents our model. Section III contains analytical results of time-dependent PDFs while Section IV provides numerical solutions. We discuss information length in Section V and entropy in Section VI. We conclude in Section VII. Appendices contain the derivation of equations used in the main text.

II. MODELS

We consider the following Langevin equation for a stochastic variable x:

$$\frac{dx}{dt} = F(x) + \xi = -\lambda(t)x - \mu x^3 + \xi. \tag{3}$$

Here,

$$F(x) = -\lambda x - \mu x^3 \tag{4}$$

is a deterministic force. x can represent any order parameter (e.g. velocity, magnetisation) and $F(x)$ is a deterministic force, which can be interpreted as the gradient of the potential $U(x)$ as $F(x) = -\frac{\partial U(x)}{\partial x}$. Thus, for FP with $F = \gamma x - \mu x^3$, $U = -\frac{\gamma}{2}x^2 + \frac{\mu}{4}x^2$ is a double well potential; for BP with $F = -\gamma x - \mu x^3$, $U = \frac{\gamma}{2}x^2 + \frac{\mu}{4}x^2$ is a mono-potential. ξ in Eq. (3) is a white noise with a short correlation time with the following statistical property:

$$\langle \xi(t)\xi(t') \rangle = 2D\delta(t - t'), \tag{5}$$

where the angular brackets denote the average over ξ, and D is the strength of the forcing. With no loss of generality, we fix the value of μ (= 1) and consider λ as a control parameter. The Fokker-Planck equation [41, 42] corresponding to Eq. (3) is as follows:

$$\frac{\partial}{\partial t}p(x,t) = \frac{\partial}{\partial x}\left[-F(x) + D\frac{\partial}{\partial x}\right]p(x,t). \tag{6}$$

Physically, $\lambda(t)$ can represent the deviation of the temperature from the critical value as $\lambda \propto T - T_c$, where T_c is the critical temperature: subcritical for $\lambda < 0$, supercritical for $\lambda > 0$, and critical at $\lambda = 0$. For $\lambda < 0$, in the absence of the stochastic noise ξ, x has the two equilibrium points $\pm\sqrt{\frac{-\lambda}{\mu}}$, while with $\xi \neq 0$, the equilibrium is described by a bimodal PDF with two peaks at $x = \pm\sqrt{\frac{-\lambda}{\mu}}$. In comparison, for $\lambda > 0$, an equilibrium PDF is unimodal with a peak at $x = 0$ when $\xi \neq 0$. Eq. (3) is motivated by Ginzburg-Landau fields in zero dimension [43], and the extension of our recent work [29, 44] on time-dependent PDF and information length for a critical state $\lambda = 0$.

In this paper, we consider a time-dependent control parameter $\lambda(t)$ such that in Forward Process (FP), λ changes from $\lambda = \gamma > 0$ to $\lambda = -\gamma < 0$, inducing disorder-to-order transition, while in Backward Process (BP), λ changes from $\lambda = -\gamma < 0$ to $\lambda = \gamma > 0$, triggering order-to-disorder transition (by definition γ is positive here). FP and BP

make up a pair of disorder-to-order and order-to-disorder transitions. A sufficiently slowly changing $\lambda(t)$ would lead to a reversible quasi-equilibrium process. In this paper, since we are interested in a far-from-equilibrium process, we introduce a sudden change λ at the beginning of FP and BP as in a quenched experiment. Specifically, we change λ from $\lambda = \gamma$ to $\lambda = -\gamma$ at $t = 0$ in FP, and from $\lambda = -\gamma$ to $\lambda = \gamma$ at $t = 0$ in BP, respectively. Alternatively, FP and BP are described by a constant λ for $t > 0$ with initial non-equilibrium PDFs as follows:

- Forward Process (FP): $\lambda = -\gamma < 0$: at $t = 0$, a unimodal PDF with a peak at $x = 0$, which evolves into a bimodal PDF with two peaks at $x = \pm\sqrt{\gamma/\mu} \neq 0$ as $t \to \infty$;
- Backward Process (BP): $\lambda = \gamma > 0$: at $t = 0$, a bimodal PDF with two peaks at $x = \pm\sqrt{\gamma/\mu} \neq 0$, which evolves into a unimodal PDF with a peak at $x = 0$ as $t \to \infty$.

FP and BP have the following equilibrium PDFs $p_F(x)$ and $p_B(x)$, respectively:

$$p_F(x) \propto \exp\Big(-\frac{\mu}{4D}(x^2 - \frac{\gamma}{\mu})^2\Big), \tag{7}$$

$$p_B(x) \propto \exp\Big(-\frac{\mu}{4D}(x^2 + \frac{\gamma}{\mu})^2\Big). \tag{8}$$

It is worth noting that for sufficiently small D, $p_F(x)$ and $p_B(x)$ can be approximated by Gaussian distributions as

$$p_F(x) \sim \frac{\sqrt{\beta_F}}{2\sqrt{\pi}}\left[e^{-\beta_F\left(x+\sqrt{\frac{\gamma}{\mu}}\right)^2} + e^{-\beta_F\left(x-\sqrt{\frac{\gamma}{\mu}}\right)^2}\right], \tag{9}$$

$$p_B(x) \sim \frac{\sqrt{\beta_B}}{\sqrt{\pi}} e^{-\beta_B x^2}, \tag{10}$$

where $\beta_F = \frac{\gamma}{D}$ and $\beta_B = \frac{\gamma}{2D}$. Eq. (9) represents the sum of the two Gaussians with peaks at $\pm\sqrt{\frac{\gamma}{\mu}}$ and variance $\frac{D}{2\gamma}$. Our FP and BP allow us to consider an interesting cyclic quenched experiment where we suddenly change λ after PDFs settle into equilibrium at the end of FP/BP, re-set time $t = 0$ and then start BP/FP process until they evolve to equilibrium, and potentially repeating indefinitely. A pair of forward/backward processes is thus completed by using $p_B(x)$ as an initial condition for FP and $p_F(x)$ for BP (see Table 1). Consequently, the initial PDFs in both FP and BP are strongly out of equilibrium, and PDFs undergo transient relaxation. We investigate time-dependent PDFs and information length during this transient relaxation, comparing them in FP and BP. In particular, we are interested in

how $\mathcal{L}$ depends on γ and D (for $\mu = 1$).

Table 1 summarizes the value of λ in Eq. (3) and initial conditions for FP and BP together with the variance $\sigma = \langle x^2 \rangle - \langle x \rangle^2$, where the angular brackets denote the average over the stochastic noise ξ. We note that p_F and p_B are equilibrium PDFs of FP and BP, respectively.

III. THEORETICAL PREDICTION OF PDFS

As will be shown later, the time evolution of PDFs in FP and BP is significantly different. It is basically because FP is dominated by the broadening of the PDF due to the stochastic noise and instability in the early stage; $x = 0$ is an unstable equilibrium point when $\xi = 0$, and the instability slowly builds up due to ξ and a finite width of the initial PDF until $t \propto O(|\ln D|)$ (see later for more details) when PDF undergoes a considerable change, developing two peaks around $x = \pm\sqrt{\gamma/\mu}$. In comparison, BP is mainly driven by the movement of the two peaks towards $x = 0$ before diffusion becomes crucial in forming a single peak at $x = 0$. In this section, we present analytical results before presenting numerical solutions in Section IV.

Case	FP	BP
$-\lambda$	γ	$-\gamma$
$p(x,0)$	$p_B(x)$	$p_F(x)$
$p(x, t \to \infty)$	$p_F(x)$	$p_B(x)$
$\sigma(t=0)$	$\frac{D}{\gamma}$	$\frac{D}{2\gamma}$
$\sigma(t \to \infty)$	$\frac{D}{2\gamma}$	$\frac{D}{\gamma}$

TABLE I: Summary of FP and BP: p_B and p_F are equilibrium PDFs of FP and BP, respectively.

A. Forward Process (FP)

FP starts with a Gaussian PDF for small D and goes through the following two stages (e.g. see [46, 47]): i) the initial stage of the broadening of the initial Gaussian PDF due to stochastic noise ξ and instability γ towards the development of the two peaks at $x = \pm\sqrt{\frac{\gamma}{\mu}}$, and ii) the final stage (Kramer's regime) of narrowing of the PDF to the final (equilibrium) (double) Gaussian PDF. To understand order formation, it is instructive to examine the evolution of PDF analytically in stage (i) in detail. To this end, it is convenient to transform away the nonlinear term in Eq. (3) into a linear damping term at the expense of a multiplicative-type stochastic noise [45]. We thus look for a variable y such that Eq. (3) becomes $dy/dt = \gamma y + \xi F(y)$ where $F(y)$ is a function of y. This is achieved by requiring $dy/dx = \gamma y/(\gamma x - \mu x^3)$, with the solution $x = y/\sqrt{1+\alpha y^2}$, where $\alpha = \frac{\mu}{\gamma}$. Specifically, y satisfies;

$$\frac{dy}{dt} = \gamma y + \xi(1+\alpha y^2)^{\frac{3}{2}}. \tag{11}$$

Eq. (11) provides a convenient way of computing y during the stage (i) by approximating $\xi(1+\alpha y^2)^{\frac{3}{2}} \sim \xi$ for small y. Thus, to leading order, y is a Gaussian process, simply given by the Ornstein–Uhlenbeck process [42] with a negative damping. The transition probability of y is therefore given by the following Gaussian PDF:

$$p(y,t;y_0,0) = \sqrt{\frac{\beta_1}{\pi}} e^{-\beta_1 (y-y_0)^2}, \tag{12}$$

where $y_0 = \frac{x_0}{\sqrt{1-\alpha x_0^2}}$ and $\frac{1}{\beta_1(t)} = \frac{D}{\gamma}(e^{2\gamma t}-1)$. In terms of y, the initial PDF $p(y,0)$ is given by

$$p(y,0) = \sqrt{\frac{\beta_0}{\pi}} e^{-\beta_0 \frac{y_0^2}{1+\alpha y_0^2}} \sim \sqrt{\frac{\beta_0}{\pi}} e^{-\beta_0 y_0^2}, \tag{13}$$

for a narrow initial PDF with $\beta_0 y_0^2 \ll 1$ (e.g. for small D). Here, $\beta_0 = \frac{1}{2\langle(\delta y_0)^2\rangle}$ is the initial inverse temperature due to the finite width of $p(x,0)$. Eqs. (12) and (13) give us

$$p(y,t) = \sqrt{\frac{\beta_0}{\pi}}\sqrt{\frac{\beta_1}{\pi}} \int_{-\infty}^{\infty} dy_0\, e^{-\beta_1 (y-y_0)^2} e^{-\beta_0 y_0^2} = \sqrt{\frac{\beta}{\pi}} e^{-\beta y^2}. \tag{14}$$

Here, $\beta = \frac{1}{2\langle(\delta y)^2\rangle}$ is the inverse temperature given by

$$\frac{1}{\beta(t)} = \frac{1}{\beta_0} e^{2\gamma t} + \frac{2D}{\gamma}(e^{2\gamma t}-1). \tag{15}$$

This can alternatively be expressed in terms of variance $\sigma = \langle (\delta y)^2 \rangle = \frac{1}{2\beta}$:

$$\sigma(t) = \frac{1}{2\beta(t)} = \sigma_0 e^{2\gamma t} + \frac{D}{\gamma}(e^{2\gamma t} - 1), \tag{16}$$

where $\sigma_0 = \frac{1}{2\beta_0} = \langle (\delta y_0)^2 \rangle = \frac{D}{\gamma}$ is the initial variance. For $t > \frac{1}{2\gamma}$, Eqs. (15) and (16) become

$$\beta \sim \frac{\gamma}{D} e^{-2\gamma t}, \quad \sigma \sim \frac{2D}{\gamma} e^{2\gamma t}. \tag{17}$$

We see from this that when D is changed to D_1 ($< D$), and simultaneously t is changed to t_1 according to

$$t_1 - t = \frac{1}{2\gamma} \ln \left[\frac{D}{D_1} \right], \tag{18}$$

that the variance remains the same. The Gaussian PDF of y in Eq. (14) is a good approximation in stage (i) before the settlement of the PDF into final equilibrium with two peaks at $x = \pm\sqrt{\frac{\gamma}{\mu}}$ in stage (ii). We now examine $p(x,t)$ corresponding to Eq. (14).

By using the conservation of the probability $p(x,t)dx = p(y,t)dy$ and Eq. (14) ($\int dy p(y,t) = 1$), we obtain the PDF of x as follows:

$$p(x,t) = \frac{1}{(1-\alpha x^2)^{\frac{3}{2}}} \sqrt{\frac{\beta}{\pi}} e^{-\beta \frac{x^2}{1-\alpha x^2}}, \tag{19}$$

which recovers the previous results [46, 47] when $\alpha = 1$. To understand the evolution of the peak of the PDF, we calculate the location x_m where PDF takes its local maximum or minimum from $\frac{\partial}{\partial x} \ln \left(p(x,t)|_{x=x_m} \right) = 0$, which satisfies

$$\alpha x_m^2 = 0, \text{ or } 1 - \frac{2\beta}{3\alpha}. \tag{20}$$

Since $\partial_{xx} \ln p(x,t) = 3\alpha - 2\beta$ at $x = 0$, $x = 0$ is a local minimum for $2\beta < 3\alpha$ while a local maximum for $2\beta > 3\alpha$. We can easily show that $x = 0$ is a local maximum at $t = 0$ since $\beta_0 = \frac{1}{2\sigma_0} = \frac{\gamma}{2D} \gg \alpha$ for small D where $\sigma_0 = \frac{D}{\gamma}$ and $\alpha = \frac{\mu}{\gamma}$. $x = 0$ remains as a local maximum until $t = t_c$ when

$$2\beta(t_c) = \frac{1}{\sigma(t_c)} = 3\alpha. \tag{21}$$

Solving Eq. (21) with the help of Eq. (16) leads to

$$t_c \sim -\frac{1}{2\gamma} \ln \left[3\alpha \left(\sigma_0 + \frac{D}{\gamma} \right) \right] \sim -\frac{1}{2\gamma} \ln \left(\frac{6D\mu}{\gamma^2} \right), \tag{22}$$

where $\sigma_0 = \frac{D}{\gamma}$, $\alpha = \frac{\mu}{\gamma}$ and $e^{2\gamma t} - 1 \sim e^{2\gamma t}$ were used for $t > \frac{1}{2\gamma}$. t_c in Eq. (22) signifies the development of a plateau at $x = 0$ due to the formation of the two peaks at $x \neq 0$ and sets the timescale beyond which Eqs. (14) and (19) cannot reasonably describe the time evolution of the PDFs. Eq. (22) demonstrates that the two peaks form at a finite time which increases with $|\ln D|$.

The formation of the two peaks discussed above is accompanied by a large (anomalous) fluctuation. That is, t_c in Eq. (22) also represents the time scale for strong fluctuations, as shall be confirmed later. We now compute second and fourth moments of x by using Eq. (14) as follows (see Appendix B):

$$\langle x^2 \rangle \;=\; \frac{2}{\alpha}\left[\frac{1}{2} - \sqrt{\frac{\beta}{\alpha}} e^{\frac{\beta}{\alpha}} \mathrm{Erfc}\left(\sqrt{\frac{\beta}{\alpha}}\right)\right], \tag{23}$$

where $\mathrm{Erfc}(Q) = \int_Q^\infty dy\, e^{-y^2} = \frac{\sqrt{\pi}}{2}\mathrm{erfc}(Q)$; $\mathrm{erfc}(Q) = \frac{2}{\sqrt{\pi}} \int_Q^\infty dy\, e^{-y^2}$ is the complementary error function. Similarly, the fourth moment is found (see Appendix C) as follows:

$$\langle x^4 \rangle \;=\; \frac{2}{\alpha^2}\left[\frac{1}{2} - \left(\frac{3}{2} + \frac{\beta}{\alpha}\right)\sqrt{\frac{\beta}{\alpha}} e^{\frac{\beta}{\alpha}} \mathrm{Erfc}\left(\sqrt{\frac{\beta}{\alpha}}\right) + \frac{\beta}{2\alpha}\right]. \tag{24}$$

In the limit of large β corresponding to small time (see Eq. (15)), we can obtain the following approximate expressions for Eqs. (23) and (24):

$$\langle x^2 \rangle \sim \frac{1}{2\beta}, \quad \langle x^4 \rangle \sim \frac{3}{4\beta^2}, \tag{25}$$

where we used the asymptotic expression

$$\mathrm{Erfc}(Q) = \frac{e^{-Q^2}}{2Q}\left[1 - \frac{1}{2Q^2} + \frac{3}{8Q^3} - \frac{15}{8Q^4} + \ldots\right] \tag{26}$$

for large Q. It is interesting to note that the value of $\langle x^2 \rangle$ and $\langle x^4 \rangle$ in Eq. (25) depending only on β is due to stochastic noise, with no dependence on the peak position $x = \pm\sqrt{1/\alpha}$. Furthermore, we observe that $\langle x^2 \rangle$ and $\langle x^4 \rangle$ are related by $\langle x^4 \rangle = 3\langle x^2 \rangle^2$, as often found in Gaussian process. This is consistent with our discussion above about stage (i) before the formation of order. In comparison, in the opposite limit of small $\beta \to 0$ for large time, we find to leading order

$$\langle x^2 \rangle \sim \frac{1}{\alpha} = \frac{\gamma}{\mu}, \quad \langle x^4 \rangle = \frac{1}{\alpha^2} = \langle x^2 \rangle^2, \tag{27}$$

which are due to the formation of two peaks at $x = \pm\sqrt{1/\alpha}$. Eqs. (25) and (27) will be confirmed by numerical simulations in Section IV.

Finally, the second and fourth moments in Eqs. (23) and (24) also play a role in determining the energy budget in the systems. To see this, we multiply Eq. (3) by x and take average over ξ and initial condition to obtain the following equation

$$\frac{1}{2}\frac{d\langle x^2\rangle}{dt} = \gamma\langle x^2\rangle - \mu\langle x^4\rangle + D. \tag{28}$$

Here, the last term D, representing the rate of energy injection by ξ, was calculated as $\langle\xi(t)x(t)\rangle = \langle\xi(t)\int_0^t dt_1[\gamma x(t_1) - \mu x(t_1)^3 + \xi(t_1)]\rangle = D$. This will be shown to be an exact result in Section IV. The middle term $\gamma\langle x^2\rangle - \mu\langle x^4\rangle \equiv H$ represents the energy into the system or environment, depending on the sign. When $H > 0$, the energy goes into the system, contributing to the increase in $\langle x^2\rangle$; when $H < 0$, the energy is dissipated in the system, increasing heat in the environment. The sign change in H will also be confirmed in Section IV. It is interesting to see from Eq. (25) that the cross-over between these two cases occurs at time when $2\beta(t_c) = 3\alpha$, which is the same as Eq. (21). Therefore, for $t < t_c$, energy goes into the system ($H > 0$) while for $t > t_c$, energy is dissipated in the system, increasing heat in the environment ($H < 0$). Thus, settling into the final equilibrium PDF involves the dissipation with $H < 0$. $H > 0$ ($H < 0$) is related to the increase (decrease) in the differential entropy in Sec. VI. Interestingly, the change in the sign of H is symptomatic of a predator-prey type self-regulating, oscillatory behaviour and is related to a geodesic, as discussed in Sec. VI.

B. Backward Process (BP)

BP starts with the initial PDF which has two peaks at $\pm\sqrt{\gamma/\mu}$, which is the final equilibrium PDF for FP. For sufficiently small D, the two peaks are far away from $x = 0$ and the PDF is approximated as the sum of the two Gaussian PDFs given by Eq. (9). The latter evolve almost independently in $x > 0$ and $x < 0$, respectively, until $t \sim O(\ln D^{-1})$ when PDFs merge and undergo significant change in the shape with large fluctuation (see Section IV). Since the evolution before merging is dominated by Gaussian evolution, the analysis becomes much simpler compared to FP. To analyze this Gaussian evolution, we can consider mean value and variance in $x > 0$ or $x < 0$ separately and treat fluctuation as small compared to the mean value. Specifically, we let $x = z + \delta x$ where $z = \langle x\rangle$ is the

mean component averaged over ξ and the initial PDF in $x > 0$ (or $x < 0$) while δx is the fluctuation $\langle \delta x \rangle = 0$. For BP, we have

$$\frac{d}{dt} z = -\gamma z - \mu z^3 - 3\mu \langle (\delta x)^2 \rangle z \sim -\gamma z - \mu z^3, \tag{29}$$

$$\frac{d}{dt} \delta x = -\gamma \delta x - 3\mu z^2 \delta x + \xi, \tag{30}$$

where the fluctuation $\langle (\delta x)^2 \rangle$ is ignored compared to the mean value z^2 in Eq. (29). By multiplying Eq. (30) by δx and then taking the average over ξ with the help of Eq. (2), we obtain the equation for the variance $\sigma \equiv \langle (\delta x)^2 \rangle$ as follows:

$$\frac{d}{dt} \sigma = -2\gamma \sigma - 6\mu z^2 \sigma + 2D. \tag{31}$$

The solutions to Eqs. (29) and (30) are as follows:

$$[z(t)]^2 = \frac{z_0^2}{(1 + \alpha z_0^2) e^{2\gamma t} - \alpha z_0^2}, \tag{32}$$

$$\sigma(t) = \frac{\sigma_0}{F'(t)} + 2D \frac{F(t)}{F'(t)}, \tag{33}$$

where $F'(t) = \left((1 + \alpha z_0^2) e^{2\gamma t} - \alpha z_0^2\right)^3 e^{-4\gamma t}$ and $F(t) = \int_0^t F'(t_1) dt_1$, $z_0 = \sqrt{\frac{\gamma}{\mu}}$, $\alpha = \frac{\mu}{\nu}$ and $\sigma_0 = \sigma(t = 0) = \frac{D}{2\gamma}$ (see Eq. (9) and Table 1). The initial evolution of PDFs in BP is dominated by the movement of the peak given by Eq. (32). As z then decreases exponentially as $z^2 \sim \frac{1}{2} z_0^2 e^{-2\gamma t}$ for $t > \frac{1}{2\gamma}$, the effect of the nonlinear term μz^2 in Eq. (31) is important only for small time $t < \frac{1}{2\gamma}$. For $t > \frac{1}{2\gamma}$, we can approximate $F'(t)$ and $F(t)$ as

$$F'(t) \sim 8 e^{2\gamma t}, \;\; F(t) \sim \frac{4}{\gamma} e^{2\gamma t}. \tag{34}$$

This, together with $\sigma_0 = \sigma(t = 0) = \frac{D}{2\gamma}$, then simplifies Eq. (33) as

$$\sigma \sim \frac{D}{\gamma}. \tag{35}$$

Since z in Eq. (32) decreases exponentially as $z^2 \sim \frac{1}{2} z_0^2 e^{-2\gamma t}$ for $t > \frac{1}{2\gamma}$, σ due to diffusion D in Eq. (35) eventually becomes important for the evolution of the PDF, say, at time $t = t_m$ when σ in Eq. (35) becomes comparable to $z^2 \sim \frac{1}{2} z_0^2 e^{-2\gamma t}$:

$$t_m \sim \frac{1}{2\gamma} \ln \left[\frac{\gamma z_0^2}{2D} \right]. \tag{36}$$

Because z and σ determine the value of different moments (e.g. $\langle x^2 \rangle = z^2 + \sigma$), the ratio of different moments (e.g. $\sqrt{\langle x^4 \rangle} / \langle x^2 \rangle$) is essentially set by t_m in Eq. (36) and is thus invariant

under the simultaneous change of t and D according to Eq. (18), as found in FP. Also, t_m increases with $\ln D^{-1}$, leading to a longer duration of the time interval where the PDF simply moves its position before D becomes important.

Eqs. (32) and (33) together with $\beta = \frac{1}{2\sigma}$ determine the evolution of the Gaussian PDF for BP as

$$p(x,t) = \frac{1}{2}\sqrt{\frac{\beta}{\pi}}\left[e^{-\beta(x-z)^2} + e^{-\beta(x+z)^2}\right]. \tag{37}$$

Eqs. (32) and (33) will also be used for computing $\mathcal{L}$ in Section V. Eq. (37) becomes invalid when the peaks start merging around $x = 0$. The merging happens when z^2 in Eq. (32) is within the variance $\frac{D}{\gamma}$ in Eq. (35) of the final PDF, roughly around $t \sim t_m$ given in Eq. (36).

IV. NUMERICAL SOLUTIONS

Without loss of generality, any finite interval in x can always be rescaled to $x \in [-1, 1]$. If the initial condition is also restricted well away from the boundaries, then solving Eq. (6) on $x \in [-1, 1]$ with boundary conditions $p = 0$ at $x = \pm 1$ is an excellent match to an unbounded interval. By rescaling t, γ and D, we can similarly fix $\mu = 1$, thereby reducing the number of parameters that need to be varied numerically to only γ and D. The numerical procedure then involves second-order finite-differencing in both space and time, using $O(10^6)$ grid-points in x, and time-steps as small as $O(10^{-7})$. Values of γ in the interval $[0, 0.7]$ were considered. The upper limit ensures that even the double-peak distribution, the final state for FP and the initial state for BP, does not encroach on the boundaries $|x| = 1$. Values of D from 10^{-3} to 10^{-7} were considered.

Figure 1 shows a simple but surprisingly useful diagnostic quantity, namely the ratio $\sqrt{\langle x^4 \rangle}/\langle x^2 \rangle$. For $D \ll 1$ this ratio is observed to be $\sqrt{3}$ for the single-peak and 1 for the double-peak, consistent with Eq. (25) and Eq. (27), respectively. FP must therefore yield $\sqrt{3} \to 1$, and BP $1 \to \sqrt{3}$. As seen in Fig. 1, the variation with D in this adjustment process is such that every reduction of D by a factor of 100 shifts the curves by a constant amount in time. That is, a time $c \ln D^{-1}$ must elapse before the ratio begins to deviate significantly from its initial value, and start the adjustment process to the other value. The numerically determined value of c is 0.71, in perfect agreement

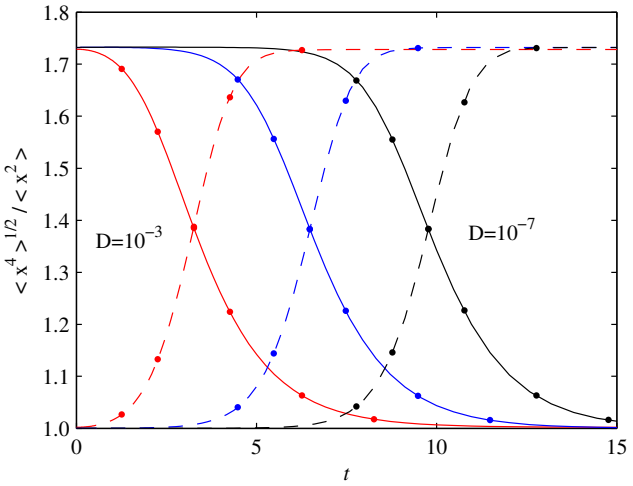

FIG. 1: (Color online) The ratio $\sqrt{\langle x^4 \rangle}/\langle x^2 \rangle$ as a function of time, for the three values $D = 10^{-3}$, 10^{-5} and 10^{-7}, from left to right as indicated. Solid lines denote FP, dashed lines BP. The dots on the lines correspond to the particular snapshots shown in Figures 2 and 3. The dots on the $D = 10^{-3}$ curves (red) are at $t = 1.26$, 2.26, 3.26, 4.26, 6.26 and 8.26; the dots on the $D = 10^{-5}$ curves (blue) are at $t = 4.48$, 5.48, 6.48, 7.48, 9.48 and 11.48; the dots on the $D = 10^{-7}$ curves (black) are at $t = 7.77$, 8.77, 9.77, 10.77, 12.77 and 14.77. The times 3.26, 6.48 and 9.77 are the values where corresponding solid and dashed lines cross; the other times are then related by fixed offsets either before or after these crossing times. Finally, $\gamma = 0.7$ for all six curves.

with the analytic prediction $\frac{1}{2\gamma} = 0.71$ from Eq. (18) for FP and Eq. (36) for BP. It is interesting that the two processes not only have the same $c \ln D^{-1}$ time shift, but even the same value of c, even though the physical origin of the shifts is so different for the two processes. In Fig. 1, the dots where corresponding solid and dashed lines cross occur at $t = 3.26,\ 6.48,\ 9.77$. This crossing time is discussed below in relation to Figs. 2 and 3.

Figure 2 shows the spatial structure of $p(x,t)$ for FP. The six snapshots correspond to the dots on the curves in Fig. 1. That is, the time shift $c \ln D^{-1}$ according to Eq. (18) is taken into account, and solutions with different values of D are compared at the times when they have the same ratios $\sqrt{\langle x^4 \rangle}/\langle x^2 \rangle$. We see that the solutions are identical for all three values of D, even though the initial conditions obviously depend strongly on D. Once the initial diffusive spreading of the central peak has occurred, the subsequent

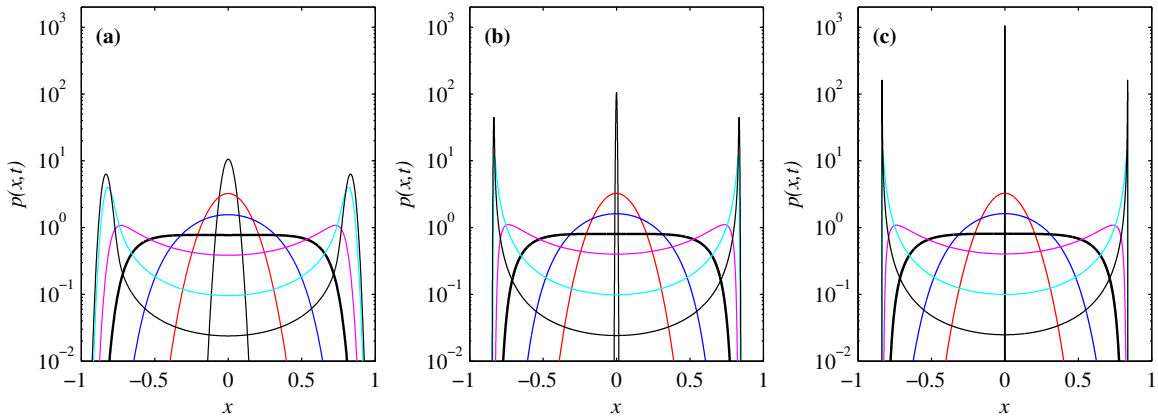

FIG. 2: (Color online) The PDFs for FP, for (a) $D = 10^{-3}$, (b) $D = 10^{-5}$, (c) $D = 10^{-7}$. The initial condition is given by the central peak. At later times this central value $p(0,t)$ monotonically decreases. The particular times shown are as indicated by the dots in Figure 1. The thick (black) lines where the central region is flattest correspond to the crossing points in Figure 1, at times 3.26 in (a), 6.48 in (b), 9.77 in (c); the times for other lines are offset relative to these values as in Figure 1. Note how the curves at intermediate times are independent of D, once this $c \ln D^{-1}$ shift in time is taken into account.

evolution is dominated by the broadening of the PDFs due to the instability (γ), and is thus independent of D. It is only at the end of the process, when the final double-peak solution is emerging, that D reasserts itself and again determines the width of the peaks.

Figure 3 shows $p(x,t)$ for BP, again at the times indicated by the dots in Fig. 1. (The evolution before these times is not shown, but was verified to be a motion of the peaks toward the origin in accordance with Eq. (32).) At these appropriately shifted times (e.g. according to Eq. (36)), the solutions are again identical and independent of D, provided that a rescaling of both x and p is now also accounted for, with x scaling as $D^{1/2}$, and p as $D^{-1/2}$. This scaling relation stems from the Gaussian evolution in Eq. (37) where $\beta \propto D^{-1}$. Note that the thick curves in Figs. 2 and 3 correspond to the times when FP and BP have the same values of $\sqrt{\langle x^4 \rangle}/\langle x^2 \rangle$ according to Fig. 1, the solid curves for FP and dashed curves for BP crossing each other. On the other hand, the PDFs in the thick curves in Fig. 2 are about to develop two peaks, suggesting that this crossing happens around the theoretically predicted time t_c in Eq. (22). By inserting numerical values of γ, $\mu = 1$, etc in Eq. (22),

we obtain $t_c = 3.1,\ 6.4,\ 9.8$ for $D = 10^{-3}$, 10^{-5} and 10^{-7}, respectively. These values are amazingly close to the numerically determined values $t = 3.26,\ 6.48,\ 9.77$ from Fig. 1, discussed above. Furthermore, the PDFs in the thick curves in Fig. 3 suggest that t_c is also close to the merging time t_m in Eq. (36). We confirm this by inserting in the parameter values in Eq. (36) as $t_m = 3.9,\ 7.2,\ 10.8$ for $D = 10^{-3}$, 10^{-5} and 10^{-7}, which are quite close to t_c.

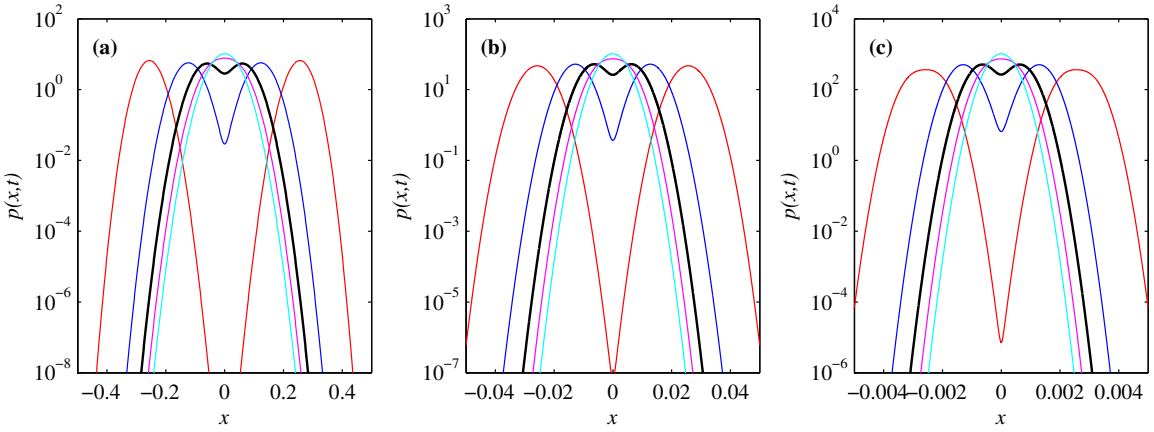

FIG. 3: (Color online) The PDFs for BP, for (a) $D = 10^{-3}$, (b) $D = 10^{-5}$, (c) $D = 10^{-7}$, at the times indicated in Figure 1. At the earliest time shown there are still two distinct peaks, which subsequently merge into one single peak. As in Figure 2, the thick (black) lines where the central region is relatively flat correspond to the crossing points in Figure 1, at times 3.26 in (a), 6.48 in (b), 9.77 in (c). The times for other lines are again offset relative to these values as in Figure 1. Note how the curves are independent of D, once the shift in time is taken into account, as well as the rescaling of x and p.

Figure 4 shows the various terms that make up the energy balance equations (28) for FP and its equivalent with $\gamma \to -\gamma$ for BP. For FP $\langle x^2 \rangle$ is monotonically increasing, hence $\frac{d}{dt}(\langle x^2 \rangle/2)$ is always positive. $\frac{d}{dt}(\langle x^2 \rangle/2)$ initially increases, driven by $\gamma\langle x^2 \rangle$, before eventually decreasing again once $\gamma\langle x^2 \rangle$ is balanced by $-\langle x^4 \rangle$. We observe the change of the sign $H = \gamma\langle x^2 \rangle - \langle x^4 \rangle$ at $t \sim t_c$ in Eq. (22). Unlike $\langle x^2 \rangle$ and $\langle x^4 \rangle$ which monotonically increase in time, the difference $\Delta = \sqrt{\langle x^4 \rangle} - \langle x^2 \rangle$ is not monotonic, but increases to its maximum before decreasing to zero as the PDF settles into its equilibrium (figure not shown). This large fluctuation Δ signifies the phase transition from disordered to ordered states due to the development of the two peaks, which occurs on time scale t_c in Eq. (22)

which increases with $\ln D^{-1}$.

It is interesting to see from Fig. 4 that the work done by the random forcing, which is the residual $\frac{d}{dt}(\langle x^2\rangle/2) - \gamma\langle x^2\rangle + \langle x^4\rangle = \langle \xi(t)x(t)\rangle$, takes the value of D for all time, in agreement with the prediction Eq. (28). This confirms that the nonlinear term does not affect the energy injection from the random forcing, on the basis of which our solutions in Section III.A were obtained. For BP, where both $-\gamma\langle x^2\rangle$ and $-\langle x^4\rangle$ are driving $\langle x^2\rangle$ toward zero, the balances are much simpler. After a very short initial phase where both damping terms are active, and $\frac{d}{dt}(\langle x^2\rangle/2)$ decreases faster than exponential, $-\gamma\langle x^2\rangle$ dominates and $\frac{d}{dt}(\langle x^2\rangle/2)$ decreases exponentially for all later times. The residual $\frac{d}{dt}(\langle x^2\rangle/2)+\gamma\langle x^2\rangle+\langle x^4\rangle = \langle \xi(t)x(t)\rangle$ is again exactly D. Finally, we note that settling to the final equilibrium takes less time in BP than in FP. For example, if we focus on when the dashed curve drops below the dotted line denoting the residual, that is, when $|\frac{d}{dt}(\langle x^2\rangle/2)| < D$, the time for this to occur in BP is consistently about 1/3 of that in FP.

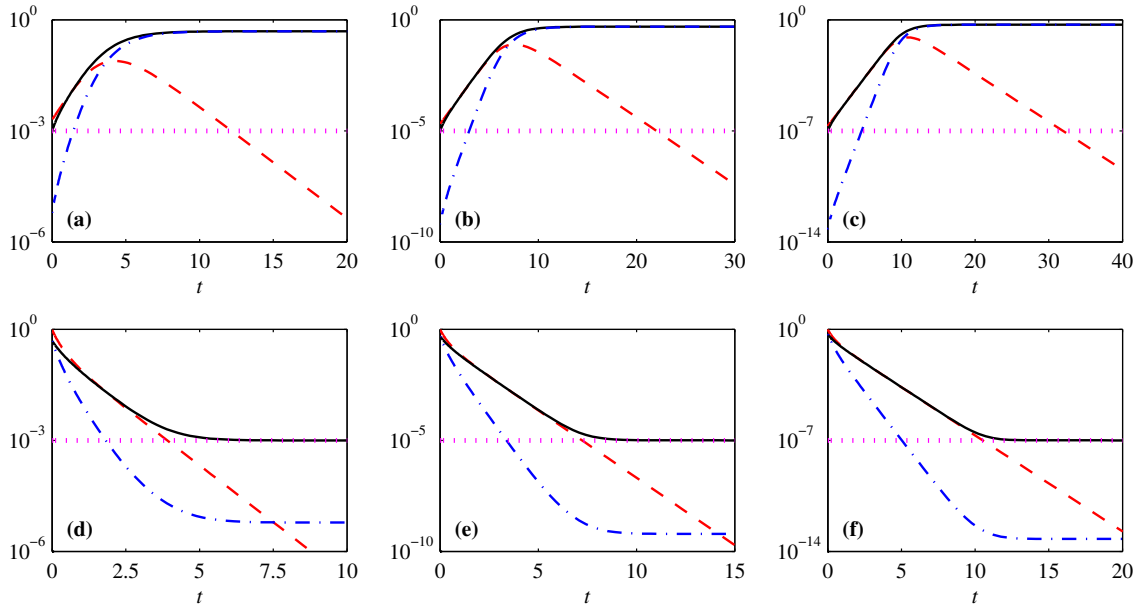

FIG. 4: The first row is for FP, with (a) $D = 10^{-3}$, (b) $D = 10^{-5}$, (c) $D = 10^{-7}$; the second row is for BP, with (d) $D = 10^{-3}$, (e) $D = 10^{-5}$, (f) $D = 10^{-7}$. Dashed curves show $|\frac{d}{dt}(\langle x^2\rangle/2)|$, solid curves $\gamma\langle x^2\rangle$, and dash-dotted curves $\langle x^4\rangle$. The dotted lines show the residuals $\frac{d}{dt}(\langle x^2\rangle/2) \mp \gamma\langle x^2\rangle + \langle x^4\rangle$, with $-$ for FP and $+$ for BP. Notice how the residuals are always exactly D.

V. INFORMATION LENGTH

Having discussed the basic dynamics of the PDFs themselves, we now elucidate the geometric structure and information change through quantities $\mathcal{E}$ and $\mathcal{L}$.

A. Forward Process

For FP, we recall the excitation of large fluctuations associated with the development of two peaks of a bimodal PDF around $t = t_c$ in Eq. (22). Since the change in $\mathcal{L}$ becomes very small for large fluctuation (i.e. large variance of a PDF) around $t = t_c$, a good estimate on the total $\mathcal{L}$ can be obtained by considering the change in $\mathcal{L}$ for i) $t < t_c$ during which our results (11)–(19) are valid with Gaussian $p(y,t)$ in Eq. (14) and for ii) $t > t_c$ when $p(x,t)$ is approximated by a Gaussian PDF with narrowing width [46]. We examine these results in detail in the following. First, for $t < t_c$, it is advantageous to compute $\mathcal{L}$ by utilising the Gaussian property of $p(y,t)$ and the invariance of $\mathcal{L}$ under the change of stochastic variables, say, x to y, as follows:

$$\begin{aligned}\mathcal{L}(t) &= \int_0^t dt_1 \sqrt{\int dx \frac{1}{p(x,t_1)}\left[\frac{\partial p(x,t_1)}{\partial t_1}\right]^2} \\ &= \int_0^t dt_1 \sqrt{\int dy \frac{1}{p(y,t_1)}\left[\frac{\partial p(y,t_1)}{\partial t_1}\right]^2} = \int_0^t dt \, \frac{1}{\tau(t)}. \end{aligned} \tag{38}$$

Here, we recall that $y = x/\sqrt{(1-\alpha x^2)}$ ($x = y/\sqrt{1+\alpha y^2}$). For the Gaussian PDFs with mean value z and variance σ, τ in Eq. (2) satisfies

$$\begin{aligned}\mathcal{E} = \frac{1}{[\tau(t)]^2} &= \frac{1}{2\beta(t)^2}\left(\frac{d\beta}{dt}\right)^2 + 2\beta\left(\frac{dz}{dt}\right)^2 \\ &= \frac{1}{2\sigma(t)^2}\left(\frac{d\sigma}{dt}\right)^2 + \frac{1}{\sigma}\left(\frac{dz}{dt}\right)^2. \end{aligned} \tag{39}$$

Here, $z = \langle y \rangle$ and $\sigma = \langle (\delta y)^2 \rangle = 1/2\beta$. Since for $t < t_c$, $\langle x^2 \rangle$ is generated by a stochastic noise (see Eq. (25)) with no mean value $\langle x \rangle = \langle y \rangle = 0$, we compute the information length in Eq. (38) by using $p(y,t)$ with the mean value $\langle y \rangle = z \sim 0$. Thus, for $t \leq t_c$ for FP, Eq. (16) and Eq. (39) with $z = 0$ give us

$$\mathcal{E} \sim 2\gamma^2 \left[\frac{\left(\sigma_0 + \frac{D}{\gamma}\right)e^{2\gamma t}}{\sigma_0 e^{2\gamma t} + \frac{D}{\gamma}(e^{2\gamma t} - 1)}\right]^2. \tag{40}$$

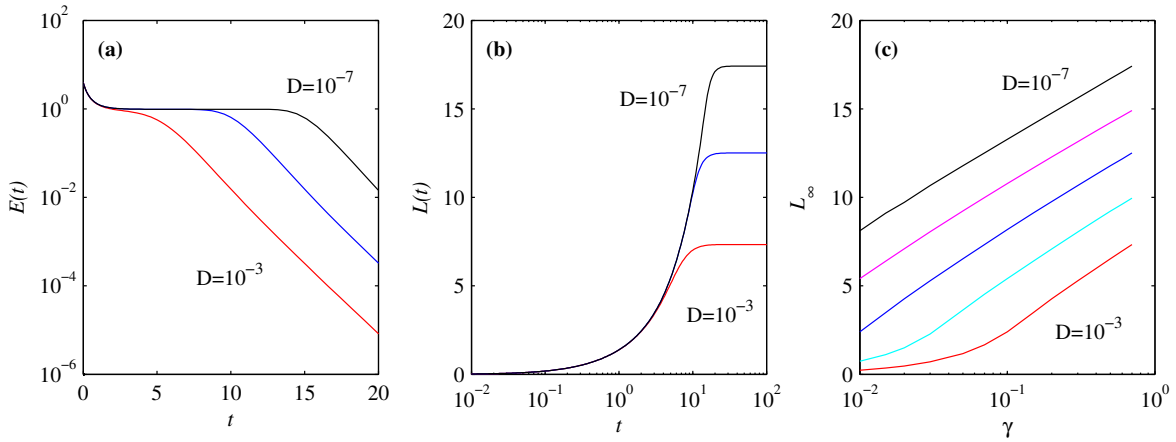

FIG. 5: (a) and (b) show $\mathcal{E}$ and $\mathcal{L}$, respectively, as functions of time, for $\gamma = 0.7$. (c) shows $\mathcal{L}_\infty$ as a function of γ. All three panels are for FP only. $D = 10^{-3}$ to 10^{-7} as indicated. Note the different combinations of linear and logarithmic scales to emphasize different features in different quantities.

By using $\sigma_0 = \sigma(t=0) = \frac{D}{\gamma}$, we obtain for small $t < \frac{1}{2\gamma}$,

$$\mathcal{E} \sim 8\gamma^2 \frac{1}{[1+2\gamma t]^2}, \tag{41}$$

while in the opposite limit $\frac{1}{2\gamma} < t < t_c$,

$$\mathcal{E} \sim 2\gamma^2. \tag{42}$$

The characteristic time of the information change $\tau = \frac{1}{\sqrt{\mathcal{E}}}$ follows from Eqs. (41) and (42). Interestingly, the constant value of $\mathcal{E}$ in Eq. (42) indicates that during this time interval, the PDF follows a geodesic. This geodesic has the characteristic time $\tau = \frac{1}{\sqrt{\mathcal{E}}} = \frac{1}{\sqrt{2}\gamma}$, reflecting that the information flow is due to the instability γ. As $t_c \propto \ln D^{-1}$, the geodesic solution persists for a longer time span for smaller D. We confirm these results in Fig. 5 which shows $\mathcal{E}(t)$, $\mathcal{L}(t)$ and $\mathcal{L}_\infty(\gamma)$. From Fig. 5a we see first that at $t = 0$, $\mathcal{E} = 3.92 = 8\gamma^2$ for all D. Furthermore, we observe a long plateau where $\mathcal{E}$ is surprisingly constant, with the value $\mathcal{E} = 2\gamma^2 = 0.98$, in perfect agreement with Eq. (42). We recall that this plateau region corresponds precisely to the intermediate stages in Fig. 1, where the ratio $\sqrt{\langle x^4 \rangle}/\langle x^2 \rangle$ is significantly different from both its initial and final values. We also see in Fig. 5a that $\mathcal{E}$ is completely independent of D up until the very final settling in to the double-peak solution, when it decreases exponentially. That $\mathcal{E}$ should be independent of D for most of the process

is consistent with our discussion in Sections III-IV, since we already saw in Fig. 2 that the entire evolution of p is independent of D. The initial diffusive broadening of the peak, which does depend on D, does not yield a D-dependent contribution to $\mathcal{E}$, agreeing with the prediction in Eq. (41).

To calculate $\mathcal{L}$, for $t < t_c$, we use Eq. (38) and Eq. (39) with $z = 0$ and obtain

$$\begin{aligned}\mathcal{L}(t_c) &\sim \frac{1}{\sqrt{2}} \ln\left(\frac{\sigma(t_c)}{\sigma_0}\right) \sim \frac{1}{\sqrt{2}} \ln\left[\frac{1}{3\alpha\sigma_0}\right] \\ &\sim \frac{1}{\sqrt{2}} \left[2\ln(\gamma) - \ln(3\mu) - \ln(D)\right]. \end{aligned} \tag{43}$$

On the other hand, during the final stage of PDF evolution in FP for $t > t_c$, the location of the two peaks does not change while the width of the PDF changes much more significantly. Thus, we can obtain a useful estimate on $\mathcal{L}$ by taking into account the change in the variance. Furthermore, since x can be approximated as a Gaussian process during this stage [46], we compute total change in $\mathcal{L}$ between t_c and $t \to \infty$ by using the result (Eq. (E9)) for the double Gaussian (see Appendix D):

$$\begin{aligned}\mathcal{L}_\infty - \mathcal{L}(t_c) &\sim \frac{1}{\sqrt{2}} \left|\ln\left(\frac{\sigma_F}{\sigma(t_c)}\right)\right| \sim \frac{1}{\sqrt{2}} \left|\ln\left[3\alpha\sigma_F\right]\right| \\ &\sim \frac{1}{\sqrt{2}} \left[2\ln(\gamma) - \ln(2\mu/3) - \ln D\right]. \end{aligned} \tag{44}$$

Here, $\sigma_F = \sigma(t \to \infty) = \frac{D}{2\gamma}$ and $\mathcal{L}_\infty = \mathcal{L}(t \to \infty)$. By adding Eqs. (43) and (44), we obtain the total $\mathcal{L}$ between the initial state at $t = 0$ and the final equilibrium state as $t \to \infty$:

$$\mathcal{L}_\infty \sim \frac{1}{\sqrt{2}} \left[4\ln(\gamma) - \ln(2\mu) - 2\ln D\right]. \tag{45}$$

Eq. (45) explicitly shows the logarithmic dependence of $\mathcal{L}$ on γ and D, as observed also in Fig. 5c. Interestingly, we can now compare Eq. (45) with the following formula that is extracted from Fig. 5c

$$\mathcal{L}_\infty \approx 0.5 + 2.2\ln\gamma - 1.1\ln D. \tag{46}$$

The coefficients of $\ln\gamma$ and $\ln D$ in Eqs. (45) and (46) are in reasonable agreement with each other. The constant term is somewhat different, but the best fit to this term is also very strongly affected by the best fit to the $\ln D$ term, since e.g. $|\ln 10^{-7}| = 16$, which is already as large as the largest $\mathcal{L}_\infty$ in Fig. 5c. The logarithmic dependence of $\mathcal{L}$ on γ

and D stems from the diffusive nature of FP with significant change in PDF width (large fluctuations).

Note also that for relatively large D and small γ the curves in Fig. 5c clearly deviate from the otherwise remarkably straight lines. This can be understood by remembering that the widths of the peaks (both single and double) scale as $D^{1/2}$, whereas the location of the double peaks is at $x = \pm\sqrt{\gamma}$. If $D \ll \gamma$ were not satisfied, the 'initial' and 'final' states would therefore already overlap so much that the entire problem becomes uninteresting. For any $\gamma > 0$ though, it is always possible to choose D small enough so that the two states are clearly distinct, and the dynamics that lead to Eq. (45) apply.

B. Backward Process

For BP, both $\mathcal{E}$ and $\mathcal{L}$ behave very differently. From Fig. 6a, we see that the initial movement of the peaks toward the origin immediately yields a very strongly D-dependent $\mathcal{E}$, since narrower peaks yield correspondingly more distinguishable states along the way (e.g. [27, 28]). This is responsible for the non-existence of a geodesic solution with constant $\mathcal{E}$. As indicated in Fig. 6b, this initial contribution to $\mathcal{L}$ then simply persists throughout the rest of the evolution, with the result that now $\mathcal{L}_\infty \propto D^{-1/2}$, so each reduction of D by a factor of 100 multiplies $\mathcal{L}_\infty$ by 10. $\mathcal{L}_\infty$ for FP and BP therefore scale completely differently with D, and for sufficiently small D it would be arbitrarily much larger for backward than forward. The variation with γ is shown in Fig. 6c, and yields $\mathcal{L}_\infty \approx 1.4\gamma D^{-1/2}$.
We now estimate $\mathcal{L}$ for BP by taking advantage of the fact that the main contribution to $\mathcal{L}$ comes from the movement of the two peaks and by using Eqs. (32) and (33):

$$\begin{aligned} \mathcal{L}(t) &\sim \int_0^t dt \frac{1}{\sigma}\frac{dz}{dt} \\ &= c_1(z_0)\int_0^t \frac{dt}{\sqrt{\sigma_0 + 2DF}}, \end{aligned} \tag{47}$$

where $c_1(z_0) = \gamma z_0 + \mu z_0^3 = 2\gamma z_0 = 2\gamma\sqrt{\frac{\gamma}{\mu}}$ ($z_0 = \sqrt{\frac{\gamma}{\mu}}$). From Eq. (47), we obtain the lower bound on $\mathcal{L}$ in the long time limit

$$\mathcal{L}_\infty \sim 2\gamma z_0 \int_0^{\frac{1}{2\gamma}} \frac{dt}{\sqrt{\sigma_0 + 2Dt}} \sim (\sqrt{6} - \sqrt{2})\frac{\gamma}{\sqrt{\mu D}}, \tag{48}$$

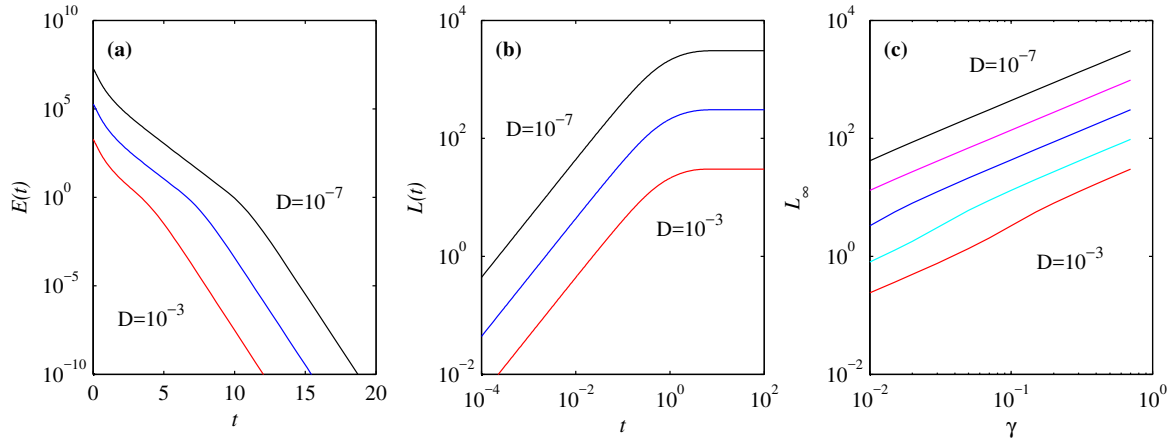

FIG. 6: (a) and (b) show $\mathcal{E}$ and $\mathcal{L}$, respectively, as functions of time, for $\gamma = 0.7$. (c) shows $\mathcal{L}_\infty$ as a function of γ. All three panels are for BP only. $D = 10^{-3}$ to 10^{-7} as indicated. Note the different combinations of linear and logarithmic scales to emphasize different features in different quantities.

where $\sigma_0 = \sigma(t = 0) = \frac{D}{2\gamma}$ for BP (see Table 1) was used. Eq. (48) explicitly shows the linear dependence of $\mathcal{L}$ on γ, as observed in Fig. 6c. Furthermore, the coefficient of 1.4 in the numerical formula agrees well with the analytic result $(\sqrt{6} - \sqrt{2}) = 1.0$, which is expected to be an underestimate. The origin of the scaling of $\mathcal{L}_\infty$ with $D^{-1/2}$ can be traced to the fact that the width of PDF ($\propto D^{-1/2}$) does not change much in BP and a statistically different state is encountered whenever the peak moves the distance of the PDF width $\propto D^{1/2}$. Similar $\mathcal{L}_\infty \propto D^{-1/2}$ was also found in both linear and cubic processes in [29]. The scaling $\mathcal{L} \propto \gamma$ essentially comes from measuring the location of the initial PDF $\propto \gamma^{1/2}$ in unit of the PDF width $\propto \gamma^{-1/2}$. Note that the contribution from $t > \frac{1}{2\gamma}$ would give scalings that are a bit more complex, as shown in Fig. 6.

VI. ENTROPY

To complement our analysis above using $\mathcal{L}$, we now look at how the (Gibbs) differential entropy $S(t) = -\int dx\, p(x,t) \ln p(x,t)$ (e.g. see [49], and using units where the Boltzmann constant $K_B = 1$) changes during the phase transition. It is important to note that S differs from $\mathcal{L}$ in that it only depends on p at any instant in time, but not on the evolution that led to that PDF. Also, we note that the differential entropy is a global measure of complexity,

independent of the rearrangement of constituent elements, and can be negative. We first compute analytically $S(t)$ for the equilibrium PDFs of FP and BP, p_F and p_B in Eqs. (7) and (8), respectively, and quantify the difference between the entropy S_F and S_B for p_F and p_B, respectively. To compute $S_F = -\int_{-\infty}^{\infty} dx\, p_F(x,t) \ln p_F(x,t)$, we express Eq. (10) as

$$p_F \;=\; \frac{\sqrt{\beta_F}}{\sqrt{\pi}} e^{-\beta_F (x^2 + x_0^2)} \cosh\left(2\beta_F x_1 x_0\right), \tag{49}$$

where $\beta_F = \gamma/D$. Then, we can show that the entropy S_F takes the following form [49]

$$S_F \;=\; \frac{1}{2}\left[1 + \ln\frac{\pi}{\beta_F}\right] + 2\beta_F x_0^2 \left[1 - \mathrm{erf}(\sqrt{\beta_F} x_0)\right] - \sqrt{\frac{\beta_F}{\pi}} 2x_0 e^{-\beta_F x_0^2} + \Delta. \tag{50}$$

Here, $\mathrm{erf}(x) = \frac{2}{\sqrt{\pi}} \int_0^x du\, e^{-u^2}$ is the error function; Δ is a function of β_F and x_0, taking the value $0 \le \Delta \le \ln 2$. For a sufficiently narrow PDF with $\beta_F x_0^2 \gg 1$, Δ was shown to take a maximum value $\ln 2$ [49]. Since in this limit $\beta_F x_0^2 \gg 1$, $\mathrm{erf}(\sqrt{\beta_F} x_0) \to 1$, Eq. (50) is simplified as

$$S_F \sim \frac{1}{2}\left[1 + \ln\frac{\pi}{\beta_F}\right] + \ln 2 = \frac{1}{2}\left[1 + \ln\frac{\pi D}{\gamma}\right] + \ln 2. \tag{51}$$

For small value of D as used in our numerical simulation, S_F is negative, signifying a strongly localised PDF.

For BF, for simplicity, we use the equilibrium p_B in Eq. (10) and $\beta_B = \frac{\gamma}{2D}$ to obtain the corresponding entropy S_B as follows:

$$S_B = -\int_{-\infty}^{\infty} dx\, p_B \ln p_B = \frac{1}{2}\left[1 + \ln\frac{2\pi D}{\gamma}\right]. \tag{52}$$

Thus, S_F in Eq. (51) is larger than S_B by $\frac{1}{2}\ln 2$ due to the formation of the two peaks.

Fig. 7 shows the time evolution of the differential entropy for FP and BP. By comparing their values at equilibrium, we see that S_F is larger than S_B by $\frac{1}{2}\ln 2$, as shown above. That is, FP and BP involve a net entropy change $\pm\frac{1}{2}\ln 2$ from one to the other. This overall change in S between FP and BP is quite small. However, Fig. 7 shows drastically different time-evolution of S in FP and BP; large increase in their value is observed around the phase transition in both processes. Also, Fig. 7 shows clearly that S behaves very differently from $\mathcal{L}$, varying most for FP, and relatively little for BP. These results can be understood by recalling from Figs. 2 and 3 that for any given D, p changes its width enormously during the

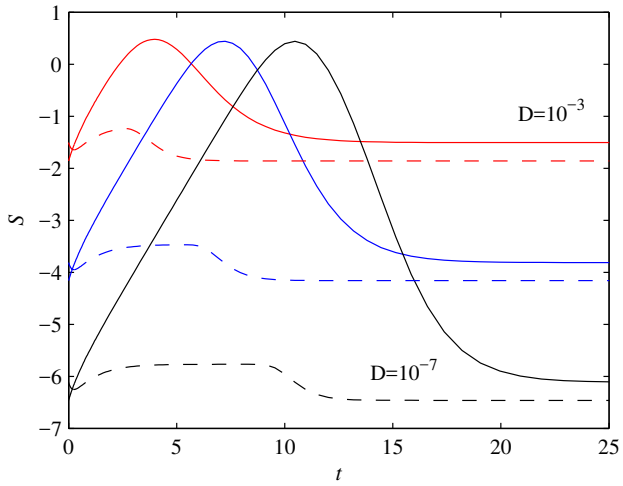

FIG. 7: The entropy S as a function of time, for the three values $D = 10^{-3}$, 10^{-5} and 10^{-7}, as indicated. Solid lines denote FP, dashed lines BP.

forward evolution, but relatively little going backward. This is reflected in S, where all three forward runs peak at the same large values of S, when the PDF is broadest, whereas the backward runs have far less variation throughout their entire evolution. The large increase in S in FP effectively reduces the number of statistically different states that a system undergoes in FP, and thus makes the total information length much smaller compared to BP. Alternatively, this result shows the emergence of order from disorder is possible through large entropy increase (also manifested by large fluctuations) in a system. The emergence of order proceeding through a high degree of disorder might be opposite to our naive expectation that the emergence of order should be an outcome of some sort of "ordered act".

The comparison of FP in Fig. 7 and Fig. 5 reveals a very interesting link between the appearance of a geodesic solution with the constant value of $\mathcal{E}$ and the large increase in $S(t)$ followed by its decrease, which is referred to as the entropy oscillation. This behaviour is reminiscent of a geodesic solution found in a non-autonomous O-U process with an oscillatory time-dependent killing term (or growth rate) together with an oscillatory time-dependent amplitude of the stochastic forcing. Note that the O-U process has a linear deterministic force and does not support a geodesic solution without a time-dependent modulation of the parameters. In sharp contrast, the linear growth rate (positive feedback) and nonlinear damping (negative feedback) in FP in our model is able to sustain a geodesic through the

predator-prey type self-regulation – the subtle energy balance between $\gamma\langle x^2\rangle$ and $\langle x^4\rangle$; the large fluctuation in $H = \gamma\langle x^2\rangle - \langle x^4\rangle$ is related to the entropy oscillation and thus the appearance of a geodesic.

VII. CONCLUSION

We investigated geometric structure during order-to-disorder and disorder-to-order transitions in a 0D Ginzburg-Landau model where the formation (disappearance) of order is modelled by the transition from a unimodal (bimodal) to bimodal (unimodal) PDF of a stochastic variable x. We considered off-critical quenching with a pair of forward and backward processes (FP and BP) for disorder-to-order and order-to-disorder transition, respectively, by choosing the initial PDF of FP/BP the same as the final equilibrium PDF of BP/FP. We demonstrated strikingly different evolution of time-dependent PDFs during transient relaxation due to non-equilibrium initial PDFs in FP and BP. In particular, FP driven by instability undergoes the broadening of the PDF with large increase in (anomalous) fluctuations before the transition to the ordered state accompanied by narrowing the PDF width. Alternatively put, the order formation in our model involves the increase in entropy followed by its decrease, that is entropy fluctuation/oscillation. In comparison, BP is mainly driven by the macroscopic motion due to the movement of the PDF peak with much less prominent appearance of a geodesic solution.

The time scale τ of the information change and the information length $\mathcal{L}_\infty = \mathcal{L}(t \to \infty)$ also behave very differently in FP and BP. In particular, FP supports an interesting geodesic solution with constant $\tau = 1/(\sqrt{2}\gamma)$, independent of the strength of the stochastic noise D, along which the information flows at the constant rate $\tau^{-1} = \sqrt{2}\gamma$. Notably, this geodesic involves the broadening followed by narrowing of a PDF (that is, the fluctuation/oscillation in PDF width) and was traced back to self-regulation between positive and negative feedback and the subtle energy balance between the linear growth and nonlinear damping in our model. Comparing with the linear O-U process where a geodesic was possible only by explicitly time-dependent model parameters, these results show that a nonlinear interaction involved in disorder-to-order transition promotes a geodesic solution. Alternatively, the self-regulation between the positive feedback (γx) and the negative feedback ($-\mu x^3$)

maintains the system closer to the geodesic, minimising the information change. In biological context, this minimal geodesic path can be understood in terms of "fitness" in the growth phase (e.g. gene expression). We suggest that the predator-prey type self-regulation between the positive feedback and the negative feedback in the disorder-to-order transition maintains the system closer to the geodesic, minimising the information change. That is, self-regulation with a nonlinear interaction facilitates a geodesic.

The total information length $\mathcal{L}_\infty$ between initial and final states is consequently much larger in BP than in FP. Specifically, it increases linearly with the deviation γ of a control parameter from the critical state in BP while increasing logarithmically with γ in FP. As $\mathcal{L}_\infty$ due to the macroscopic motion is a more useful form of the energy that can be extracted, a larger $\mathcal{L}_\infty$ in BP than in FP suggests the possibility of extracting a net useful energy from a pair of FP and BP processes, e.g. in a cyclic order-disorder transition, often observed in nature. On the other hand, from the perspective of the fitness of a system discussed above and in Sec. I, a smaller $\mathcal{L}$ in FP can be considered to be advantageous for the system when adjusting to a changing environment takes time and/or is costly. Furthermore, we showed that $\mathcal{L}$ has the great capability of capturing different physical processes – diffusion/advection involved in FP/BP – by geometry. In particular, $\mathcal{L}_\infty \propto |\ln D|$ and $D^{-1/2}$ in FP and BP, respectively reveal drastically different roles of diffusion D in FP/BP transition.

Finally, we note that order-to-disorder transition always occurred faster than disorder-to-order transition, as often observed in self-organising systems. These results suggest that a cyclic order-disorder transition in our toy model could serve as a useful simple model to capture dynamic equilibrium in self-organising systems which maintain a quasi-equilibrium, repeating the formation and disappearance of a coherent structure. Building upon the understanding of our 0D model within which a detailed mathematical analysis was possible, it would be of great interest to extend this model to a more realistic case (e.g. 1D or 2D model, a system of coupled equations, etc).

Appendix A: Relation between $\mathcal{L}$ and relative entropy

We first show the relation between $\tau(t)$ in Eq. (2) and the second derivative of the relative entropy (or Kullback-Leibler divergence) $D(p_1, p_2) = \int dx\, p_2 \ln(p_2/p_1)$ where $p_1 = p(x, t_1)$ and $p_2 = p(x, t_2)$ as follows:

$$\frac{\partial}{\partial t_1} D(p_1, p_2) = -\int dx p_2 \frac{\partial_{t_1} p_1}{p_1}, \tag{A1}$$

$$\frac{\partial^2}{\partial t_1^2} D(p_1, p_2) = \int dx p_2 \left[\frac{(\partial_{t_1} p_1)^2}{p_1^2} - \frac{\partial_{t_1}^2 p_1}{p_1} \right], \tag{A2}$$

$$\frac{\partial}{\partial t_2} D(p_1, p_2) = \int dx \left[\partial_{t_2} p_2 + \partial_{t_2} p_2 (\ln p_2 - \ln p_1) \right], \tag{A3}$$

$$\frac{\partial^2}{\partial t_2^2} D(p_1, p_2) = \int dx \left[\partial_{t_2}^2 p_2 + \frac{(\partial_{t_2} p_2)^2}{p_2} + \partial_{t_2}^2 p_2 (\ln p_2 - \ln p_1) \right]. \tag{A4}$$

By taking the limit where $t_2 \to t_1 = t$ ($p_2 \to p_1 = p$) and by using the total probability conservation (e.g. $\int dx \partial_t p = 0$), Eqs. (A1) and (A3) above lead to

$$\lim_{t_2 \to t_1 = t} \frac{\partial}{\partial t_1} D(p_1, p_2) = \lim_{t_2 \to t_1 = t} \frac{\partial}{\partial t_2} D(p_1, p_2) = \int dx \partial_t p = 0, \tag{A5}$$

while Eqs. (A2) and (A4) give

$$\lim_{t_2 \to t_1 = t} \frac{\partial^2}{\partial t_1^2} D(p_1, p_2) = \lim_{t_2 \to t_1 = t} \frac{\partial^2}{\partial t_2^2} D(p_1, p_2) = \int dx \frac{(\partial_t p)^2}{p}. \tag{A6}$$

See also [38] for similar derivation.

To link this to information length $\mathcal{L}$, we then express $D(p_1, p_2)$ for small $dt = t_2 - t_1$ as

$$D(p_1, p_2) = \frac{1}{2} \left[\int dx \frac{(\partial_{t_1} p(x, t_1))^2}{p} \right] (dt)^2 + O((dt)^3), \tag{A7}$$

where $O((dt)^3)$ is higher order term in dt. We define the infinitesimal distance (information length) $dl(t_1)$ between t_1 and $t_1 + dt$ by

$$dl(t_1) = \sqrt{D(p_1, p_2)} = \frac{1}{\sqrt{2}} \sqrt{\int dx \frac{(\partial_t p)^2}{p}} dt + O((dt)^{3/2}). \tag{A8}$$

The total change in information between time $t = 0$ and t is then obtained by summing over $dt(t_1)$ and taking the limit $dt \to 0$ as

$$\begin{aligned} \mathcal{L}(t) &= \lim_{dt \to 0} [dl(0) + dl(dt) + dl(2dt) + dl(3dt) + \cdots dl(t - dt)] \\ &= \lim_{dt \to 0} \left[\sqrt{D(p(x,0), p(x,dt))} + \sqrt{D(p(x,dt), p(x,2dt))} + \cdots \sqrt{D(p(x,t-dt), p(x,t))} \right] \\ &\propto \int_0^t dt_1 \sqrt{\int dx \frac{(\partial_{t_1} p)^2}{p}}. \end{aligned} \tag{A9}$$

Appendix B: Derivation of Eqs. (7)-(10)

To find the equilibrium PDFs $p_F(x)$ and $p_B(x)$, we look for the stationary solution of the Fokker-Planck equation Eq. (6);

$$0 = \frac{\partial}{\partial t}p(x,t) = \frac{\partial}{\partial x}\left[-F(x) + D\frac{\partial}{\partial x}\right]p(x,t), \tag{B1}$$

and find that

$$p(x, t\to\infty) \propto \exp\Big(-\frac{1}{D}\int^x dx_1 F(x_1)\Big). \tag{B2}$$

For FP, $F(x) = -\gamma x + \mu x^3$, and thus

$$p(x,t\to\infty) = p_F \propto \exp\Big(-\frac{1}{4D}\left[2\gamma x^2 - \mu x^4\right]\Big) \propto \exp\Big(-\frac{\mu}{4D}\left[x^2 - \frac{\gamma}{\mu}\right]^2\Big), \tag{B3}$$

For BP, $F(x) = \gamma x + \mu x^3$, and thus

$$p(x,t\to\infty) = p_F \propto \exp\Big(-\frac{1}{4D}\left[2\gamma x^2 + \mu x^4)\right]\Big) \propto \exp\Big(-\frac{\mu}{4D}\left[x^2 + \frac{\gamma}{\mu}\right]^2\Big). \tag{B4}$$

For sufficiently small D, we can approximate $p_F(x)$ by expanding it around the two peaks $x = \pm\sqrt{\frac{\gamma}{\mu}}$. Specifically, around $x = \sqrt{\frac{\gamma}{\mu}}$,

$$\left[x^2 - \frac{\gamma}{\mu}\right]^2 = \left[x - \sqrt{\frac{\gamma}{\mu}}\right]^2\left[x + \sqrt{\frac{\gamma}{\mu}}\right]^2 \sim 4\frac{\gamma}{\mu}\left[x - \sqrt{\frac{\gamma}{\mu}}\right]^2. \tag{B5}$$

Similarly, around $x = -\sqrt{\frac{\gamma}{\mu}}$,

$$\left[x^2 - \frac{\gamma}{\mu}\right]^2 = \left[x - \sqrt{\frac{\gamma}{\mu}}\right]^2\left[x + \sqrt{\frac{\gamma}{\mu}}\right]^2 \sim 4\frac{\gamma}{\mu}\left[x + \sqrt{\frac{\gamma}{\mu}}\right]^2. \tag{B6}$$

Thus, these results enable us to approximate $p_F(x)$ by the double Gaussian given by Eq. (9) in the text. For BP, for small D, the PDF has a narrow peak around $x = 0$. Thus, by neglecting x^4 in Eq. (8) in comparison with x^2, we obtain Eq. (10).

Appendix C: Derivation of Eq. (23)

In order to compute the second moment, we utilise $p(x,t)dx = p(y,t)dy$:

$$\begin{aligned}\langle x^2\rangle &= \int_{-\infty}^{\infty} dx\, p(x,t)x^2 = \int_{-\infty}^{\infty} dy\, p(y,t)x^2 = \int_{-\infty}^{\infty} dy\, x^2\sqrt{\frac{\beta}{\pi}}e^{-\beta y^2}\\ &= 2\int_0^{\infty} dy\frac{y^2}{1+\alpha y^2}\sqrt{\frac{\beta}{\pi}}e^{-\beta y^2}\\ &= \frac{2}{\alpha}\left[\frac{1}{2} - \sqrt{\frac{\beta}{\pi}}I\right]\end{aligned} \tag{C1}$$

where the integral $I \equiv \int_0^\infty \frac{1}{1+\alpha y^2} e^{-\beta y^2}$. In Eq. (C1), $\mathrm{Erfc}(Q) = \int_Q^\infty dy\, e^{-y^2} = \frac{\sqrt{\pi}}{2}\mathrm{erfc}(Q)$ where $\mathrm{erfc}(Q) = \frac{2}{\sqrt{\pi}} \int_Q^\infty dy\, e^{-y^2}$ is the complementary error function. In order to compute $I \equiv \int_0^\infty \frac{1}{1+\alpha y^2} e^{-\beta y^2}$, we differentiate I with respect to β and obtain the following differential equation;

$$\begin{aligned} \partial_\beta I &= -\int_0^\infty dy \frac{y^2}{1+\alpha y^2} e^{-\beta y^2} \\ &= -\frac{1}{\alpha}\left[\frac{1}{2}\sqrt{\frac{\beta}{\pi}} - \int_0^\infty \frac{1}{1+\alpha y^2} e^{-\beta y^2}\right] \\ &= -\frac{1}{2\alpha}\sqrt{\frac{\beta}{\pi}} + \frac{1}{\alpha} I. \end{aligned} \tag{C2}$$

Thus,

$$\partial_\beta I - \frac{1}{\alpha} I = -\frac{1}{2\alpha}\sqrt{\frac{\beta}{\pi}}. \tag{C3}$$

We solve Eq. (C3) as

$$I(\beta) = I(\beta_0) e^{\frac{\beta}{\alpha}} - \sqrt{\frac{\pi}{2\alpha}} e^{\frac{\beta}{\alpha}} J, \tag{C4}$$

where $\beta_0 = 0$ and

$$\begin{aligned} I(\beta_0) &= \int_0^\infty \frac{1}{1+\alpha y^2} = \frac{\pi}{2\sqrt{\alpha}}, \\ J &= \int_{\beta_0}^{\beta} \frac{d\beta_1}{\sqrt{\beta_1}} e^{\frac{-\beta_1}{\alpha}}. \end{aligned} \tag{C5}$$

J in Eq. (C5) is calculated as follows:

$$\begin{aligned} J &= 2\int_0^{\sqrt{\beta}} e^{-\frac{z^2}{\alpha}} \\ &= 2\sqrt{\alpha}\int_0^{\sqrt{\frac{\beta}{\alpha}}} dp\, e^{-p^2} \\ &= \sqrt{\alpha\pi} - 2\sqrt{\alpha}\mathrm{Erfc}\left(\sqrt{\frac{\beta}{\alpha}}\right). \end{aligned} \tag{C6}$$

By substituting Eq. (C6) in Eq. (C4), we obtain

$$I = \sqrt{\frac{\pi}{\alpha}} e^{\frac{\beta}{\alpha}} \mathrm{Erfc}\left(\sqrt{\frac{\beta}{\alpha}}\right). \tag{C7}$$

By inserting Eq. (C7) in Eq. (C1), we obtain

$$\langle x^2 \rangle = \frac{2}{\alpha}\left[\frac{1}{2} - \sqrt{\frac{\beta}{\alpha}} e^{\frac{\beta}{\alpha}} \mathrm{Erfc}\left(\sqrt{\frac{\beta}{\alpha}}\right)\right], \tag{C8}$$

which is Eq. (23) in Section III.

Appendix D: Derivation of Eq. (24)

In order to compute the fourth moment, we again utilise $p(x,t)dx = p(y,t)dy$:

$$\begin{aligned}\langle x^4\rangle &= \int_{-\infty}^{\infty} dy\, p(y,t)x^4 = \int_{-\infty}^{\infty} dy\, x^4 \sqrt{\frac{\beta}{\pi}} e^{-\beta y^2} \\ &= 2\int_0^{\infty} dy \frac{y^4}{(1+\alpha y^2)^2}\sqrt{\frac{\beta}{\pi}} e^{-\beta y^2} \\ &= \frac{2}{\alpha^2}\left[\frac{1}{2} + \sqrt{\frac{\beta}{\pi}}(-2I+K)\right] \end{aligned} \tag{D1}$$

where $K \equiv \int_0^{\infty} \frac{1}{(1+\alpha y^2)^2} e^{-\beta y^2}$. To evaluate $K \equiv \int_0^{\infty} \frac{1}{(1+\alpha y^2)^2} e^{-\beta y^2}$, we rewrite I by using $\alpha = \gamma/\mu$ as

$$I = \gamma \int_0^{\infty} \frac{1}{\gamma + \mu y^2} e^{-\beta y^2}, \tag{D2}$$

and consider

$$\begin{aligned}\partial_\gamma \left(\frac{I}{\gamma}\right) &= \partial_\gamma \int_0^{\infty} \frac{1}{\gamma+\mu y^2} e^{-\beta y^2} \\ &= -\frac{1}{\gamma^2}\int_0^{\infty} \frac{1}{(1+\alpha y^2)^2} e^{-\beta y^2}. \end{aligned} \tag{D3}$$

Eq. (D3) gives

$$K = -\gamma^2 \partial_\gamma \left(\frac{I}{\gamma}\right). \tag{D4}$$

We rewrite I/γ by using $\alpha = \gamma/\mu$

$$\begin{aligned}\frac{I}{\gamma} &= \sqrt{\frac{\pi}{\mu\gamma}} e^{\frac{\beta\gamma}{\mu}} \mathrm{Erfc}\left(\sqrt{\frac{\beta\gamma}{\mu}}\right) \\ &= \sqrt{\frac{\pi}{\mu\gamma}} e^{\frac{\beta\gamma}{\mu}} \int_{\sqrt{\beta\gamma/\mu}}^{\infty} dp\, e^{-p^2}. \end{aligned} \tag{D5}$$

We then obtain from Eq. (D5):

$$\partial_\gamma \left(\frac{I}{\gamma}\right) = \left(-\frac{1}{2\gamma} + \frac{\beta}{\mu}\right)\frac{I}{\gamma} - \frac{1}{2\gamma\mu}\sqrt{\beta\pi}. \tag{D6}$$

Using Eq. (D6) in (D1) gives us

$$\langle x^4\rangle = \frac{2}{\alpha^2}\left[\frac{1}{2} - \left(\frac{3}{2} + \frac{\beta}{\alpha}\right)\sqrt{\frac{\beta}{\alpha}} e^{\frac{\beta}{\alpha}} \mathrm{Erfc}\left(\sqrt{\frac{\beta}{\alpha}}\right) + \frac{\beta}{2\alpha}\right], \tag{D7}$$

which is Eq. (24) in the text.

Appendix E: Properties of the sum of two Gaussian PDFs

In this Appendix, we show that the information length for double Gaussian PDFs which are well-separated is approximately the same as that for a single Gaussian PDF. To this end, we let

$$\begin{aligned} p &= p_1 + p_2 = N(t)[\tilde{p}_1 + \tilde{p}_2], \\ N(t) &= \frac{\sqrt{\beta(t)}}{2\sqrt{\pi}}, \\ \tilde{p}_1 &= e^{-\beta(t)(x+x_0)^2} = e^{-\beta(t)x_1^2}, \\ \tilde{p}_2 &= e^{-\beta(t)(x-x_0)^2} = e^{-\beta(t)x_2^2}. \end{aligned} \tag{E1}$$

Here, N is the normalisation constant (e.g. $N^{-1} = \int dx(\tilde{p}_1 + \tilde{p}_2)$) and $x_1 = x + x_0$ and $x_2 = x - x_0$.

To show Eq. (44), we assume x_0 is constant given by the peak location $x_0 = \sqrt{\frac{\gamma}{\mu}}$ in $x > 0$ while $\beta = \beta(t)$ depending on time. Then, we can show

$$\frac{1}{p(x,t)}\left[\frac{\partial p(x,t)}{\partial t}\right]^2 = \frac{\dot{N}^2}{N}(\tilde{p}_1 + \tilde{p}_2) + 2\dot{N}(\dot{\tilde{p}}_1 + \dot{\tilde{p}}_2) + N\frac{(\dot{\tilde{p}}_1 + \dot{\tilde{p}}_2)^2}{\tilde{p}_1 + \tilde{p}_2}. \tag{E2}$$

Now, we compute the various quantities in Eq. (E2) as follows:

$$\begin{aligned} \dot{\tilde{p}}_1 &= -\dot{\beta}x_1^2\tilde{p}_1 = \dot{\beta}\partial_\beta\tilde{p}_1, \\ (\dot{\tilde{p}}_1)^2 &= \dot{\beta}^2\tilde{p}_1\partial_{\beta\beta}\tilde{p}_1. \end{aligned} \tag{E3}$$

Similarly,

$$\begin{aligned} \dot{\tilde{p}}_2 &= -\dot{\beta}x_2^2\tilde{p}_2 = \dot{\beta}\partial_\beta\tilde{p}_2, \\ (\dot{\tilde{p}}_2)^2 &= \dot{\beta}^2\tilde{p}_2\partial_{\beta\beta}\tilde{p}_2. \end{aligned} \tag{E4}$$

Thus, by using Eqs. (E3) and (E4), we calculate the last term in Eq. (E2) as follows:

$$(\dot{\tilde{p}}_1 + \dot{\tilde{p}}_2)^2 = \dot{\beta}^2\left[\tilde{p}_1\partial_{\beta\beta}\tilde{p}_1 + \tilde{p}_2\partial_{\beta\beta}\tilde{p}_2 + 2\partial_\beta\tilde{p}_1\partial_\beta\tilde{p}_2\right] \tag{E5}$$

$$= \dot{\beta}^2\left[(\tilde{p}_1 + \tilde{p}_2)\partial_{\beta\beta}\tilde{p}_1 + (\tilde{p}_1 + \tilde{p}_2)\partial_{\beta\beta}\tilde{p}_2 + G_1\right] \tag{E6}$$

$$= \dot{\beta}^2\left[(\tilde{p}_1 + \tilde{p}_2)\partial_{\beta\beta}(\tilde{p}_1 + \tilde{p}_2) + G_2\right], \tag{E7}$$

where G_1 and G_2 are terms involving the product of $\tilde{p}_1$ and $\tilde{p}_2$. For the PDF peaks that are well-separated and thus independent, there is no overlap between $\tilde{p}_1$ and $\tilde{p}_2$ in x, leading to

$\int dx \tilde{p}_1(x)\tilde{p}_2(x) = 0$. That is, in this case, $\int dx\, G_1 = \int dx\, G_2 = 0$. Thus, these terms G_1 and G_2 do not contribute to Eq. (2). By using these results in Eq. (2), we obtain

$$\int dx \frac{1}{p(x,t)} \left[\frac{\partial p(x,t)}{\partial t}\right]^2 = \frac{\dot{N}^2}{N^2} + 2\dot{\beta}\dot{N}\partial_\beta \frac{1}{N} + N\dot{\beta}^2 \partial_{\beta\beta}\frac{1}{N}. \tag{E8}$$

By using $N = \frac{1}{2}\sqrt{\frac{\beta}{\pi}}$, we simplify Eq. (E8) as

$$\int dx \frac{1}{p(x,t)} \left[\frac{\partial p(x,t)}{\partial t}\right]^2 = \frac{\dot{\beta}^2}{2\beta^2} = \frac{\dot{\sigma}^2}{2\sigma^2}. \tag{E9}$$

Thus, Eq. (E9) is the same as Eq. (39) in the limit $z = 0$. We note that Eq. (44) is obtained by the time integral of Eq. (E9).

Next to show Eq. (47), we need to consider the case where β is constant in Eq. (E1) while $x_0 = x_0(t)$ depends on time. In this case, we have

$$\begin{aligned}(\dot{\tilde{p}}_1 + \dot{\tilde{p}}_2)^2 &= 4\beta^2 \dot{x_0}^2 N^2 \left[x^2(\tilde{p}_1 + \tilde{p}_2)^2 + 2x x_0(\tilde{p}_1^2 - \tilde{p}_2^2) + x_0^2(\tilde{p}_1 - \tilde{p}_2)^2\right] \\ &= 4\beta^2 \dot{x_0}^2 N^2 \left[x^2(\tilde{p}_1 + \tilde{p}_2)^2 + 2x x_0(\tilde{p}_1^2 - \tilde{p}_2^2) + x_0^2(\tilde{p}_1 + \tilde{p}_2)^2 + G_3\right], \end{aligned} \tag{E10}$$

where G_3 is a function depending on the product of $\tilde{p}_1$ and $\tilde{p}_2$, which vanishes upon integration over x when $\tilde{p}_1$ and $\tilde{p}_2$ are well-separated with negligible overlap. In this case,

$$\begin{aligned}\int dx \frac{1}{p(x,t)} \left[\frac{\partial p(x,t)}{\partial t}\right]^2 &= 4\beta^2 \dot{x_0}^2 N \int dx \left[(x + x_0)^2 \tilde{p}_1 + (x - x_0)^2 \tilde{p}_2\right] \\ &= -4\beta^2 \dot{x_0}^2 N \partial_\beta \int dx\, (\tilde{p}_1 + \tilde{p}_2) \\ &= -4\beta^2 \dot{x_0}^2 N \partial_\beta \frac{1}{N} \\ &= 2\beta \dot{x_0}^2, \end{aligned} \tag{E11}$$

where we used $N = \frac{1}{2}\sqrt{\frac{\beta}{\pi}}$ and thus $\partial_\beta \frac{1}{N} = -\frac{1}{2\beta N}$. Eq. (E11) is the same as Eq. (39) in the opposite limit where $z = x_0$ and $\dot{\beta} = 0$.

Appendix F: Two independent Gaussian PDFs

It is interesting to consider what would happen in the case of the broken ergodicity such that the PDFs in $x > 0$ and $x < 0$ are independent. To this end, we recast Eq. (10) as

$$\begin{aligned} p_F &= \frac{1}{2}\left[p_1 + p_2\right], \\ p_1 &= \frac{\sqrt{\beta_F}}{\sqrt{\pi}} e^{-\frac{\gamma}{D}\left(x+\sqrt{\frac{\gamma}{\mu}}\right)^2}, \\ p_2 &= \frac{\sqrt{\beta_F}}{\sqrt{\pi}} e^{-\frac{\gamma}{D}\left(x-\sqrt{\frac{\gamma}{\mu}}\right)^2}, \end{aligned} \tag{F1}$$

where $\beta_F = \gamma/D$ and compute the configurational entropy [50] by taking into account the probability of $1/2$ of x to be in $x > 0$ or $x < 0$ as follows:

$$S_{Fc} = -\frac{1}{2}\int_{-\infty}^{\infty} dx\, \left[p_1 \ln p_1 + p_2 \ln p_2\right] = -\int_{-\infty}^{\infty} dx\, p_1 \ln p_1 = -\frac{1}{2}\left[1 + \ln\frac{\pi D}{\gamma}\right], \tag{F2}$$

where we used $\int_{-\infty}^{\infty} dx\, p_1 \ln p_1 = \int_{-\infty}^{\infty} dx\, p_2 \ln p_2$ due to symmetry under $x \to -x$. Interestingly, Eqs. (51) and (F2) differ by $\ln 2$ due to the broken ergodicity (i.e. due to the reduction of a phase space by half). This difference of $\ln 2$ is however negligible for small D and $S_F \sim S_{Fc} \sim -\frac{1}{2}\ln\frac{\pi D}{\gamma}$. On the other hand, S_{Fc} in Eq. (F2) taking into account the breakdown of ergodicity is smaller than S_B by $\frac{1}{2}\ln 2$ as the ergodic phase region is reduced to $x > 0$ or $x < 0$. Again, this difference is very small compared to the contribution from D.

---

[1] T.W.B. Kibble, Phys. Rep., **67**, 183 (1980).

[2] Y. Nagashima, Elementary Particle Physics: Quantum Field Theory and Particles, Vol. 1, (John Wiley & Sons, 2011).

[3] G. Mazenko, Physica A, **204** 437 (1994).

[4] G. Longo and M Montévil, Progress in Biophysics and Molecular Biology. Systems Biology and Cancer. **106**, 340 (2011)

[5] T. Bossomaier, R. Barnett and M. Harré, Complex Adaptive Systems Modeling, **1**, 1 (2013).

[6] H. Haken, Information and Self-organization: A macroscopic approach to complex systems, 3rd Ed., Springer (2006).

[7] E. Kim and P.H. Diamond, Phys. Rev. Lett., **90**,185006 (2003).

[8] E. Kim, Phys. Rev. Lett., **96**, 084504 (2006).

[9] K. Srinivasan and W.R. Young, J. Atmos. Sci., **69**, 1633 (2012).

[10] K.M. Sayanagi, A.P. Showman and T.E. Dowling, Jour. Atmos. Sci., **65**, 12 (2008).

[11] E. Kim, H. Liu and J. Anderson, Phys. Plasmas, **16**. 0552304 (2009).

[12] A.P.L. Newton, E. Kim and H.-L. Liu, Phys. Plasmas, **20**, 092306 (2013).

[13] M. Tsuchiya, A. Giuliani, M. Hashimoto, J. Erenpreisa and K. Yoshikawa, PLoS One, **10**, e0128565 (2015).

[14] C. Tang and P. Bak, J. Stat. Phys. 51, 797 (1988).

[15] H. J. Jensen, Self-organized criticality: emergent complex behavior in physical and biological systems (Cambridge university press, Cambridge, 1998).

[16] G. Pruessner, Self-organised criticality (Cambridge Univ. Press, Cambridge, 2012).

[17] S. Fauve and F. Heslot, Phys. Lett. A, **97**, 5 (1983).

[18] M.L. Ferguson, D. Le Coq, M. Jules, S. Aymerich, O. Radulescue, N. Declerck and C.A. Royer, PNAS, **109**, 155 (2012).

[19] D. Angeli, J. E. Ferrell, and E. D. Sontag, PNAS **101**, 1822 (2004).

[20] D. Holcman and M. Tsodyks, PLoS Comp Biol **2**, e23 (2006).

[21] J. F. Mejias, H. J. Kappen, and J. J. Torres, PLoS One **5**, e13651 (2010).

[22] J. Hidalgo, L. F. Seoane, J. M. Coŕtes, and M. A. Munoz, PloS One **7**, e40710 (2012).

[23] S. Tyagi, Mol. Syst. Biol. **11**, 805 (2015).

[24] S. di Santo, R. Burioni, A. Vezzani, and M.A. Muñoz, Phys. Rev. Lett. **116**, 240601 (2016).

[25] S.B. Nicholson and E. Kim, Phys. Lett. A., **379**, 8388 (2015).

[26] S.B. Nicholson and E. Kim, Entropy, **18**, 258, e18070258 (2016).

[27] J. Heseltine and E. Kim, J. Phys. A **49**, 175002 (2016).

[28] E. Kim, U. Lee, J. Heseltine and R. Hollerbach, Phys. Rev. E **93**, 062127 (2016).

[29] E. Kim and R. Hollerbach, Phys. Rev. E, **95**, 022137 (2017).

[30] A.L. Gibbs and F.E. Su, Int. Stat. Rev. **70**, 419 (2002).

[31] W.K. Wootters, Phys. Rev. D, **23**, 357 (1981).

[32] G. Ruppeiner, Phys. Rev. A., **20**, 1608 (1979).

[33] F. Schlögl, Z. Phys. B – Cond. Matt., **59**, 449 (1985).

[34] E.H. Feng and G.E. Crooks, Phys. Rev. E., **79**, 012104 (2009).

[35] S.L. Braunstein and C.M. Caves, Phys. Rev. Lett., **72**, 3439 (1994).

[36] H. Strobel, W. Muessel, D. Linnemann, T. Zibold, D.B. Hume, L. Pezzé, A. Smerzi, M.K. Oberthaler, Science, **345**, 424 (2014).

[37] J. Nulton, P. Salamon, B. Andresen and Qi. Anmin, J Chem. Phys., **83**, 334 (1985).

[38] G.E. Crooks, Phys. Rev. Lett., **99**, 100602 (2007).

[39] D.A. Sivak and G.E. Crooks Phys. Rev. Lett. **8**, 190602 (2012).

[40] P. Salamon. J.D. Nulton, G. Siragusa, A. Limon, D. Bedeaus and S. Kjelstrup, J. Non-Equilib. Thermodyn., **27**, 45 (2002).

[41] F. Klebaner, Introduction to Stochastic Calculus with Applications, Imperial College Press (2012).

[42] H. Risken, The Fokker-Planck Equation: Methods of Solutions and Applications, 3rd Ed. Springer (2013).

[43] J.K. Bhattacharjee, P. Meakin and D.J. Scalapino, Phys. Rev. A. **30**, 1026 (1984).

[44] E. Kim and R. Hollerbach, Phys. Rev. E, **94**, 052118 (2016).

[45] M. Suzuki, Phys. Lett. A, 339 **67**, (1978).

[46] M. Suzuki, Prog. Theo. Phys., **77**, 477 (1976); J. Stat. Phys., **16**, 11 (1977).

[47] B. Caroli, C. Caroli and B. Roulet, J. Stat. Phys., **21**, 415 (1979).

[48] R. Kubo, K. Matsuo and K. Kitahara, J. Stat. Phys., **9**, 51 (1973).

[49] J.V. Michalowicz, J.M. Nichols and F. Bucholtz, Entropy, **10**, 200 (2008).

[50] J.C. Mauro, R.J. Loucks and S. Sen, J. Chem. Phys., **133**, 164503 (2010).